Lithos 198–199 (2014) 281–297

Contents lists available at ScienceDirect

Lithos

journal homepage: www.elsevier.com/locate/lithos

Origin of gem corundum in calcite marble: The Revelstoke occurrence in the Canadian Cordillera of British Columbia

Tashia J. Dzikowski [a,*], Jan Cempírek [a,b], Lee A. Groat [a], Gregory M. Dipple [a], Gaston Giuliani [c]

[a] Department of Earth, Ocean and Atmospheric Sciences, University of British Columbia, 2207 Main Mall, Vancouver, BC V6T 1Z4, Canada
[b] Department of Mineralogy, Moravian Museum, Zelný trh 6, Brno 61137, Czech Republic
[c] IRD et CRPG/CNRS, Centre de Recherches Pétrographiques et Géochimiques, 15 rue Notre Dame des Pauvres, Vandoeure-lés-Nancy 54501, France

ARTICLE INFO

Article history:
Received 30 July 2013
Accepted 31 March 2014
Available online 12 April 2014

Keywords:
Corundum
Muscovite
Calcite marble
Oxygen isotopes
Geochemistry
Metamorphism

ABSTRACT

The calcite marble-hosted gem corundum (ruby, sapphire) occurrence near Revelstoke, British Columbia, Canada, occurs in the Monashee Complex of the Omineca Belt of the Canadian Cordillera. Corundum occurs in thin, folded and stretched layers with green muscovite + Ba-bearing K-feldspar + anorthite ($An_{0.85-1}$) ± phlogopite ± Na-poor scapolite. Other silicate layers within the marble are composed of: (1) diopside + tremolite ± quartz and (2) garnet ($Alm_{0.7-0.5}Grs_{0.2-0.4}$) + Na-rich scapolite + diopside + tremolite + Na,K-amphiboles. Non-silicate layers in the marble are either magnetite- or graphite-bearing. Predominantly pink (locally red or purple) opaque to transparent corundum crystals have elevated Cr_2O_3 (≤0.21 wt.%) and variable amounts of TiO_2; rare blue rims on the corundum crystals contain higher amounts of TiO_2 (≤0.53 wt.%) and Fe_2O_3 (≤0.07 wt.%). The associated micas have elevated Cr, V, Ti, and Ba contents. Petrography of the silicate layers show that corundum formed from muscovite at the peak of metamorphism (~650–700 °C at 8.5–9 kbar). Because the marble is almost pure calcite (dolomite is very rare), the corundum was preserved because it did not react with dolomite to spinel + calcite during decompression. The scapolite-bearing assemblages formed during or after decompression of the rock at ~650 °C and 4–6 kbar. Gem-quality corundum crystals formed especially on borders of the mica-feldspar layers in an assemblage with calcite.

Whole rock geochemistry data show that the corundum-bearing silicate (mica-feldspar) layers formed by mechanical mixing of carbonate with the host gneiss protolith; the bulk composition of the silicate layers was modified by Si and Fe depletion during prograde metamorphism. High element mobility is supported by the homogenization of $\delta^{18}O$ and $\delta^{13}C$ values in carbonates and silicates for the marble and silicate layers. The silicate layers and the gneiss contain elevated contents of Cr and V due to the volcanoclastic component of their protolith.

1. Introduction

The origin of gem corundum (Al_2O_3), which includes ruby (red variety, Cr,V-bearing) and sapphire (blue and other colors), has recently been the subject of significant interest due to the growing economic potential of the gem corundum market, new deposits, and advances in understanding of their origin (e.g., reviews of Giuliani et al., 2007; Groat and Laurs, 2009; Simonet et al., 2008). Ruby and sapphire are arguably the world's most widely sold colored gemstones, accounting for approximately one-third of sales by value (BUZ Consulting 2009, in Shor and Weldon, 2009), and commanding some of the highest prices paid for any gem.

Corundum only forms in Al-rich assemblages deficient in Si; in order to form ruby and sapphire, chromophores such as Cr, V, Ti, and Fe must also be present. The enrichment in both Al and Cr is problematic because both are relatively insoluble and difficult to transport over large distances in aqueous solutions that are poor in Si (Manning, 2007). Several showings of gem corundum have been described in Canada (Fig. 1A), including: blue, yellow, and colorless sapphire near Kimmirut on Baffin Island (discovered in 2002; Gertzbein, 2005; LeCheminant et al., 2005); sapphire in southeastern Newfoundland (discovered in 1987; Wight, 1999); "low-grade ruby" near Sydney, Nova Scotia (discovered in 2004; Durstling, 2005); sapphire from eastern Ontario (Wight, 2004); and star sapphire from several localities near Passmore in south-central British Columbia (discovered in the early 1980s; Wilson, 2010).

A new carbonate-hosted gem corundum locality northwest of Revelstoke in British Columbia (at 51° 31.3′ N, 118° 46.7′ W, 82M/10; Fig. 1) was staked as the Goat claims by Bradley S. Wilson in 2002. Several gem-quality sapphires and rubies from this locality have been faceted with the largest under 0.5 ct. (Appendix A, Suppl. Fig. A1). In

* Corresponding author.
E-mail address: t.dzikowski@alumni.ubc.ca (T.J. Dzikowski).

http://dx.doi.org/10.1016/j.lithos.2014.03.030
0024-4937/

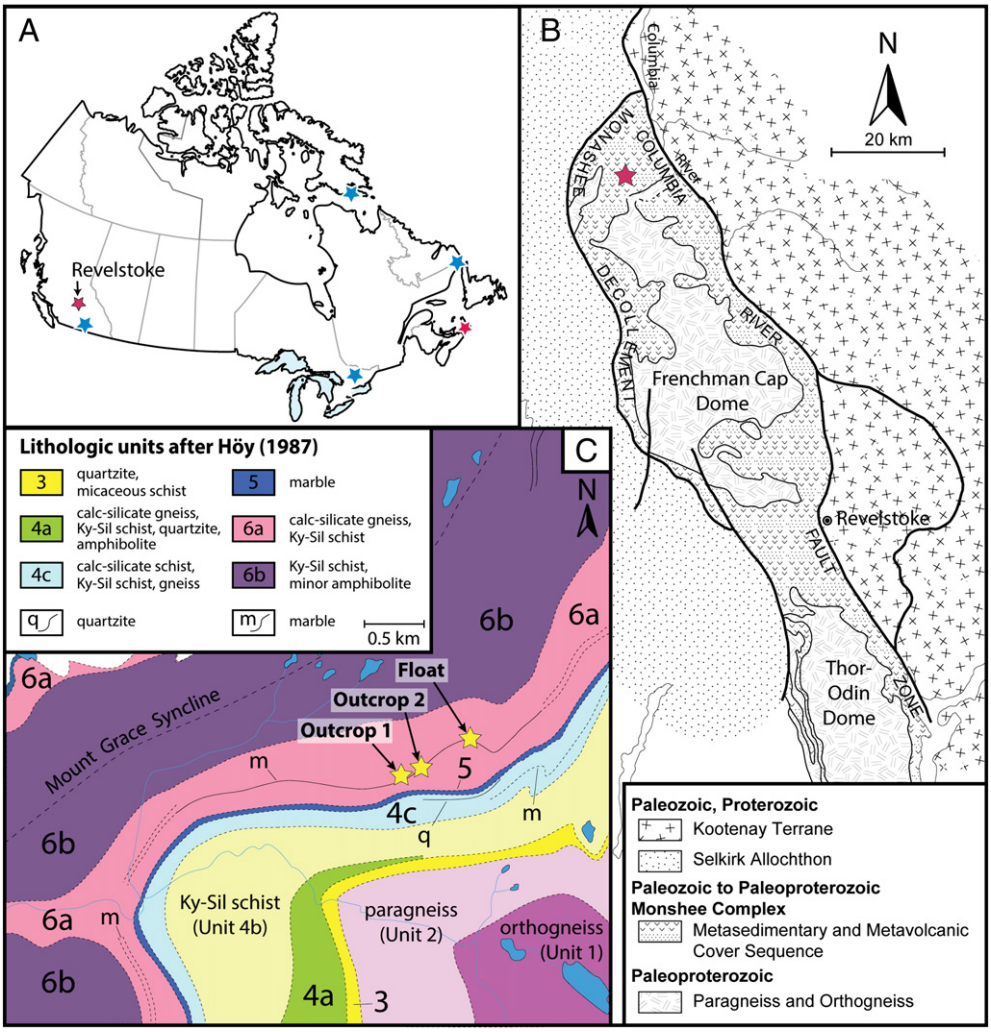

Fig. 1. Location and geology of the Revelstoke occurrence. A) Map showing Canadian gem-corundum localities. B) Tectonic assemblage of part of the Monashee complex. The studied area is marked with a star. C) Regional geological map of the Revelstoke occurrence (Units 1–6 are marked by numbers). The studied locations (from east to west: float, outcrop 1, outcrop 2) are marked with yellow stars.
Panel b is modified after Höy (2001). Panel c is modified after Höy (1987).

this contribution we characterize the geology, geochemistry, mineralogy, and fluid inclusions found in the corundum at the Revelstoke locality in order to draw conclusions about the genesis of this occurrence.

2. Geological setting

The Revelstoke occurrence is located in the Shuswap Metamorphic Core Complex (MCC), in the southern part of the Omineca Belt of the Canadian Cordillera in British Columbia. It is hosted in a marble layer within the Monashee Complex cover sequence northwest of the Frenchman Cap dome (Fig. 1). The Omineca Belt is a northwest trending uplifted region of metamorphic and plutonic rocks separating accreted terranes from the ancestral North America continental margin in the Canadian Cordillera (Johnson, 2006). Rocks within the Omineca Belt are typically highly deformed and variably metamorphosed. The Shuswap MCC is the most deeply exhumed part of the southern Omineca Belt in the core of the Canadian Cordillera (Johnson, 2006). The Monashee Complex is the lowest exposed part of the Shuswap MCC and is the largest exposure of Precambrian crystalline rocks in the Canadian Cordillera (Crowley, 1999). The Monashee Complex, which contains the Frenchman Cap dome to the north and the Thor–Odin dome to the south (Fig. 1B), is bounded by the Monashee décollement in the west and the Columbia River fault in the east (Brown, 1980; Brown et al., 1986; Crowley, 1999; Johnson, 2006; Journeay, 1986).

During the formation of the Frenchman Cap and Thor–Odin domes, initial compressional tectonism was succeeded by extension of the orogen along the Columbia River and Okanagan–Eagle River fault system following a path of isothermal decompression and isobaric cooling. The exact mechanism of decompression and uplift is discussed by Teyssier et al. (2005), Hinchey et al. (2006), Gervais et al. (2010), and Gervais and Brown (2011). All suggest similar P–T paths with peak metamorphic conditions of ca. 750–800 °C and 8–10 kbar followed by isothermal decompression to <5 kbar and isobaric cooling to 300–150 °C. The observed inverted metamorphic gradient in the northern part of the Frenchman Cap dome (Journeay, 1986) was explained by Crowley and Parrish (1999) as a juxtaposition of high-grade rocks over a lower-grade metapelitic rock sequence with regular metamorphic zonation. The Monashee décollement was active during both Mesozoic orogenesis (Read and Brown, 1981) and early Tertiary (~58 Ma) extension and uplift (Lane, 1984). Work by Crowley and Parrish (1999) shows that the pelitic schist, which borders the marble hosting the Revelstoke occurrence, has thermal peak U–Pb monazite and zircon ages that range from 57 to 51 Ma.

3. Lithological units of the Monashee complex

The Monashee complex contains Paleoproterozoic to Cambrian shallow marine metasedimentary cover rocks up to 2–3 km thick which uncomformably overlay a core of Paleoproterozoic basement migmatitic paragneiss and granitoid orthogneiss rocks (Crowley, 1999; Crowley et al., 2001). Höy (1987) suggested that the marble-hosting metapelitic sedimentary sequence in the northern part of the Frenchman Cap dome was deposited on a shallow marine shelf to intertidal platform environment. He interpreted the scapolite-bearing metapelitic assemblages as former muds and silts with varying amounts of carbonate that were deposited under saline conditions, with halite as a possible constituent of the original sedimentary rock.

According to Höy (1987), the stratigraphic succession of autochthonous cover rocks above the basement gneiss is divided into three units (Fig. 1C): the lower assemblage (Unit 3, quartzite), the middle assemblage (Unit 4, calcareous and pelitic schists with the extrusive Mount Grace carbonatite, and Unit 5, marble), and the upper assemblage (Unit 6a, b, calcareous and pelitic schist). The Revelstoke gem corundum occurrence occurs in a marble layer within the upper assemblage (Unit 6a).

The upper assemblage is divided into two parts. Unit 6a contains interlayered light gray to green scapolite-bearing calc-silicate gneiss and sillimanite schist, an impure marble (which hosts the corundum), and the Cottonbelt sulfide–magnetite layer, which is interpreted as a sedimentary-exhalative (SEDEX) deposit with some features of Broken Hill-type deposits (Höy, 2001). Unit 6b contains interlayered sillimanite schist, quartz feldspar gneiss, thin chert, and impure quartzite layers (Höy, 1987).

4. Methods

Representative polished thin sections of host metapelites, marble, and corundum-bearing calc-silicate layers within marble were studied using optical and scanning electron microscopy (SEM) and cathodoluminescence (CL) microscope to characterize the minerals and determine the paragenetic sequence.

Whole rock major and trace element analyses of the major rock types were done at ALS Chemex in Vancouver using a combination of ICP-AES and ICP-MS for major and trace elements (package CCP-PKG01). Chondrite normalization after Sun and McDonough (1989) is used for data presentation.

A detailed description of the analytical methods for ^{40}Ar–^{39}Ar (Renne et al., 1998; Ludwig, 2003) dating is given in Appendix B.

Chemical compositions of minerals were determined using a fully automated CAMECA SX-50 electron microprobe, operating in the wavelength-dispersion mode with the following operating conditions: excitation voltage, 15 kV; beam current, 20 nA; peak count time, 20 s; background count-time, 10 s; spot diameter, 2–5 μm. Data reduction was done using the 'PAP' $\phi(\rho Z)$ method (Pouchou and Pichoir, 1985).

Table 1
Representative corundum compositions (electron microprobe analyses).

	G10-1	G022C-17-1	ZC-15	G014B1-7
Color	Pink	Pink	Blue	Blue
TiO_2 wt.%	0.09	0.13	0.53	0.37
Al_2O_3	99.68	99.51	98.17	98.58
V_2O_3	0.01	0.06	0.01	0.03
Cr_2O_3	0.21	0.08	b.d.l.	0.11
Fe_2O_3	0.04	0.04	0.03	0.07
MgO	b.d.l.	b.d.l.	0.02	0.02
Total	100.03	99.82	98.76	99.17

b.d.l. = below detection limit. Contents of Mn were below detection limit. The following standards, X-ray lines and crystals were used: rutile, TiKa, PET; corundum, AlKa, TAP; metallic V, VKa, PET; synthetic magnesiochromite, CrKa, LIF; synthetic fayalite, FeKa, LIF; diopside, MgKa, TAP. Detection limits for V and Cr: 0.01 wt.% V_2O_3, 0.02 wt.% Cr_2O_3.

The standards used are listed the in tables containing the analytical data for each mineral (Table 1, and Appendix C).

Carbon and oxygen stable isotopic composition of both phosphoric acid leach-separated (carbonate and silicate) and drill-separated mineral samples (corundum and calcite) were determined in three different laboratories. The results are given relative to VPBD and VSMOW.

Leach-separated carbonate and drill-separated calcite mineral samples were analyzed at the Pacific Centre of Isotopic and Geochemical Research at UBC in Vancouver, Canada. Analyses were carried out using the gas bench and a Delta PlusXL mass spectrometer in continuous flow mode. Samples were acidified with 99% phosphoric acid in helium-flushed sealed vials, and the headspace gas was measured in a helium flow. The $\delta^{13}C$ (VPDB) and $\delta^{18}O$ (VSMOW) results were based on an average of multiple analyses of NBS-18 and -19 standards. The analyses were corrected for fractionation using repeated analyses of UBC internal carbonate standards BN 13, BN 83-2, and H6M, which were previously calibrated against NBS-18 and -19.

Carbonate drill powder analyses were performed at UBC using the Mineral Deposit Research Unit Mineral Isotope Analyzer (Barker et al., 2011). Samples were acidified with 85% phosphoric acid in sealed, non-flushed glass vials and the headspace gas was measured. The analyses were corrected for fractionation using repeated analyses of UBC internal carbonate standards BN 13, BN 83-2, and H6M, which were previously calibrated against NBS-18 and -19.

Leach-separated carbonate and silicate analyses were performed at Queen's Facility for Isotope Research, Queen's University, Canada. Carbonates were dissolved in phosphoric acid and $^{18}O/^{16}O$ ratios were measured from the released CO_2; a BF_5 extraction line was used for oxygen in silicates. Analyses were carried out using the Finnigan GasBench II and a Finnigan MAT 252 isotope-ratio mass spectrometers. The analytical procedure was analogous to that used by Uvarova et al. (2011).

Corundum $\delta^{18}O$ analyses were performed using the method described by Giuliani et al. (2005). Only unaltered corundum grains embedded in calcite were analyzed.

Mineral abbreviations used follow Whitney and Evans (2010).

5. Geology and petrography of the corundum occurrence

The corundum-bearing marble is exposed for several kilometers along strike within Unit 6a (Fig. 1C) and is bounded on both sides by a heterogeneous gneiss with metapelitic layers. The boundaries between the marble and the host gneiss are sharp, but intercalations of the marble with gneiss layers at the boundaries are common. The host rocks and the marble are extensively folded.

Rock samples were obtained from boulders of marble float (locality "float") with common corundum and green muscovite, as well as from two marble outcrops — one with common green muscovite and rare corundum (locality "outcrop 1"), and second with common scapolite and rare corundum and muscovite (locality "outcrop 2"; Fig. 1C). Samples of gneiss and various layers in marble (diopside, magnetite, graphite, and garnet) were collected from the outcrops. A sample of tourmaline in a medium-grained marble was collected between the float locality and outcrop 1.

5.1. Marble

The marble is composed of fine- to medium-grained calcite; only very rare dolomite was observed at the contact with the host rock and as microscopic inclusions in calcite within the magnetite-rich layers. The calcite matrix contains impure siliceous and non-siliceous laminations and layers, generally parallel to the contact. The siliceous layers can be divided into three contrasting types: (1) mica-feldspar-bearing (with corundum; Fig. 2A); (2) diopside–tremolite-bearing; and very rare (3) diopside–garnet–amphibole–scapolite-bearing. The non-siliceous layers are graphite- and/or magnetite-bearing (Fig. 2B). The graphite layers are more common than the siliceous ones, and the

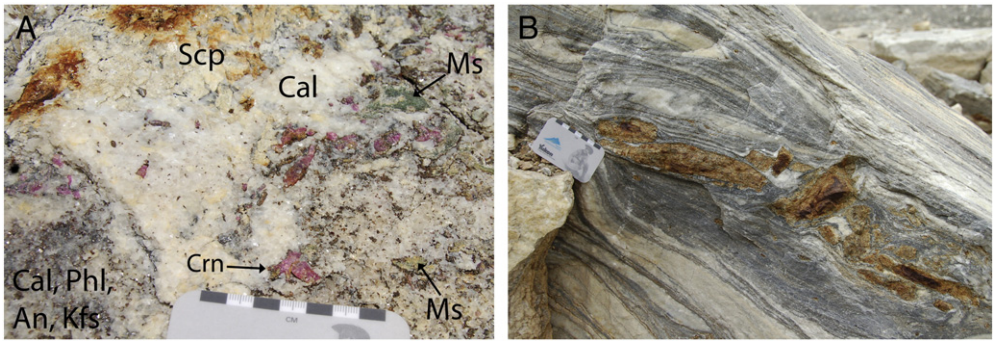

Fig. 2. Rock photographs of the Revelstoke occurrence. A) Corundum-bearing mica-feldspar layers, with secondary scapolite after anorthite; B) altered fragments of deformed muscovite-feldspar layers enclosed in calcite, together with phlogopite and graphite layers in marble.
Mineral abbreviations after Whitney and Evans (2010).

magnetite layers are relatively rare. The marble is commonly folded, with boudins and broken grains of feldspars and scapolite enclosed in deformed mica-feldspar-bearing layers. The marble locally shows evidence of post-metamorphic pressure-induced calcite grain boundary migration recrystallization and cataclasis. Rare cross-cutting calcite veins with deformed coarse-grained carbonate crystals in a fine-grained matrix have been observed.

5.1.1. Mica-feldspar-rich layers

Mica-feldspar-rich layers with minor corundum (Fig. 2A) are dispersed throughout the marble unit and individual layers can be traced for several tens of meters on the outcrop surface. They range in thickness from 1 to 20 cm and are thickest near the contact with the host gneiss. The grain size ranges from ~0.1 to 40 mm. The layers are foliated, and they are commonly folded and boudinaged (Fig. 2B).

The layers are locally mineralogically zoned (Fig. 3); they contain green muscovite aggregates rimmed by anorthite, K-feldspar, phlogopite, and corundum (zone 1), which are enclosed by calcite + phlogopite ± plagioclase ± K-feldspar ± corundum (zone 2). The surrounding calcite layers (zone 3) rarely contain crystals of corundum or aggregates of anorthite + K-feldspar + muscovite, which are isolated from the adjacent silicate layer due to shearing of the marble. Zones 1 and 2 sometimes contain minor amounts of scapolite; zones 2 and 3 may also contain accessory quartz. Corundum can occur in all three zones, but it has never been seen in contact with quartz.

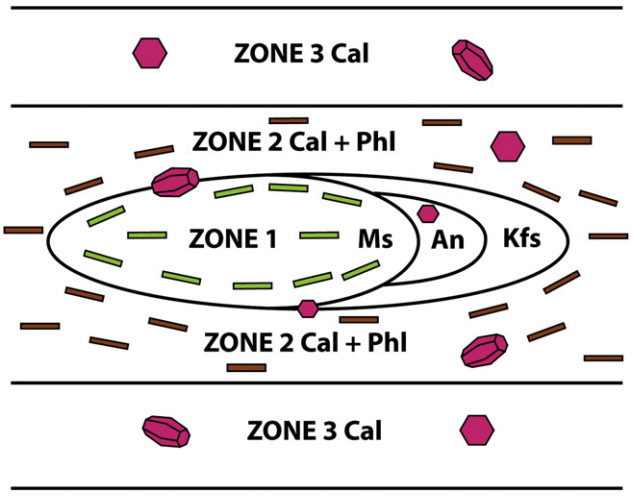

Fig. 3. Schematic drawing of mineralogical zoning in the marble and in the mica-feldspar layers. The pink symbols represent randomly oriented corundum crystals.

Zone 1 contains deformed lensoidal aggregates of green muscovite which are commonly rimmed by phlogopite, anorthite, K-feldspar and minor corundum (Figs. 2A, 3, 4A–D). Anorthite and K-feldspar usually contain common inclusions of coarse-grained phlogopite, muscovite and calcite, and minor rutile and apatite. Muscovite aggregates contain only minor fine-grained phlogopite, rutile, apatite and rare zircon and Th-rich uraninite (Fig. 4A–D). K-feldspar is generally later than anorthite but in some cases the feldspars are intergrown. K-feldspar grains are commonly zoned with Ba-enriched rims (Fig. 4C). Phlogopite in the marble is rarely overgrown by muscovite. Pseudomorphs after titanite are locally present as an assemblage of rutile + K-feldspar + anorthite ±calcite ± titanite in the muscovite aggregates. Where large rutile inclusions are in contact with calcite or anorthite, newly formed titanite is rarely observed.

Zone 2 is characterized by calcite with dispersed phlogopite, anorthite, K-feldspar, and minor aggregates of anorthite and K-feldspar with relict muscovite. Accessory phases present in this zone are corundum, scapolite, and rutile, along with trace amounts of apatite, Fe-oxide, graphite ± quartz ± pyrite. Scapolite locally occurs as isolated anhedral grains replacing anorthite, or as euhedral crystals in sulfide-filled pockets in carbonate veinlets.

Zone 3 marble layers contain calcite ± trace quartz ± apatite ± euhedral corundum. The calcite in the marble layers is mostly coarse-grained (0.5–2 mm), although it is locally rimmed by fine-grained calcite (<0.1 mm) as a result of recrystallization. Apatite and quartz occur with the fine-grained calcite, but their crystals are rounded and not recrystallized.

Corundum occurs in three morphological types: (1) euhedral, sometimes zoned crystals or crystal fragments enclosed in Zone 1 within feldspars or muscovite aggregates (Fig. 4D, E); (2) euhedral zoned corundum with calcite inclusions, enclosed in calcite or in feldspar on the border of muscovite aggregates (Zones 2 and 3; Fig. 4F); and (3) fine-grained aggregates of corundum with very common inclusions of rutile and apatite, enclosed in feldspar or calcite (Zones 2 and 3; Fig. 4G). The euhedral type (1) forms crystals ~3–10 mm in diameter, with minor euhedral inclusions of rutile, apatite and rare zircon; in mica-feldspar aggregates it locally encloses grains of muscovite and Ba-rich K-feldspar. Rare inclusions of anorthite were found in anorthite-rimmed corundum (Fig. 4E). In phlogopite-rich mica-feldspar layers, corundum may enclose phlogopite crystals. The euhedral corundum type (2) forms large crystals up to 3 cm long and 1 cm wide, with an average width of 5–10 mm, sometimes with typical hexagonal dipyramids. The corundum crystals usually contain rounded

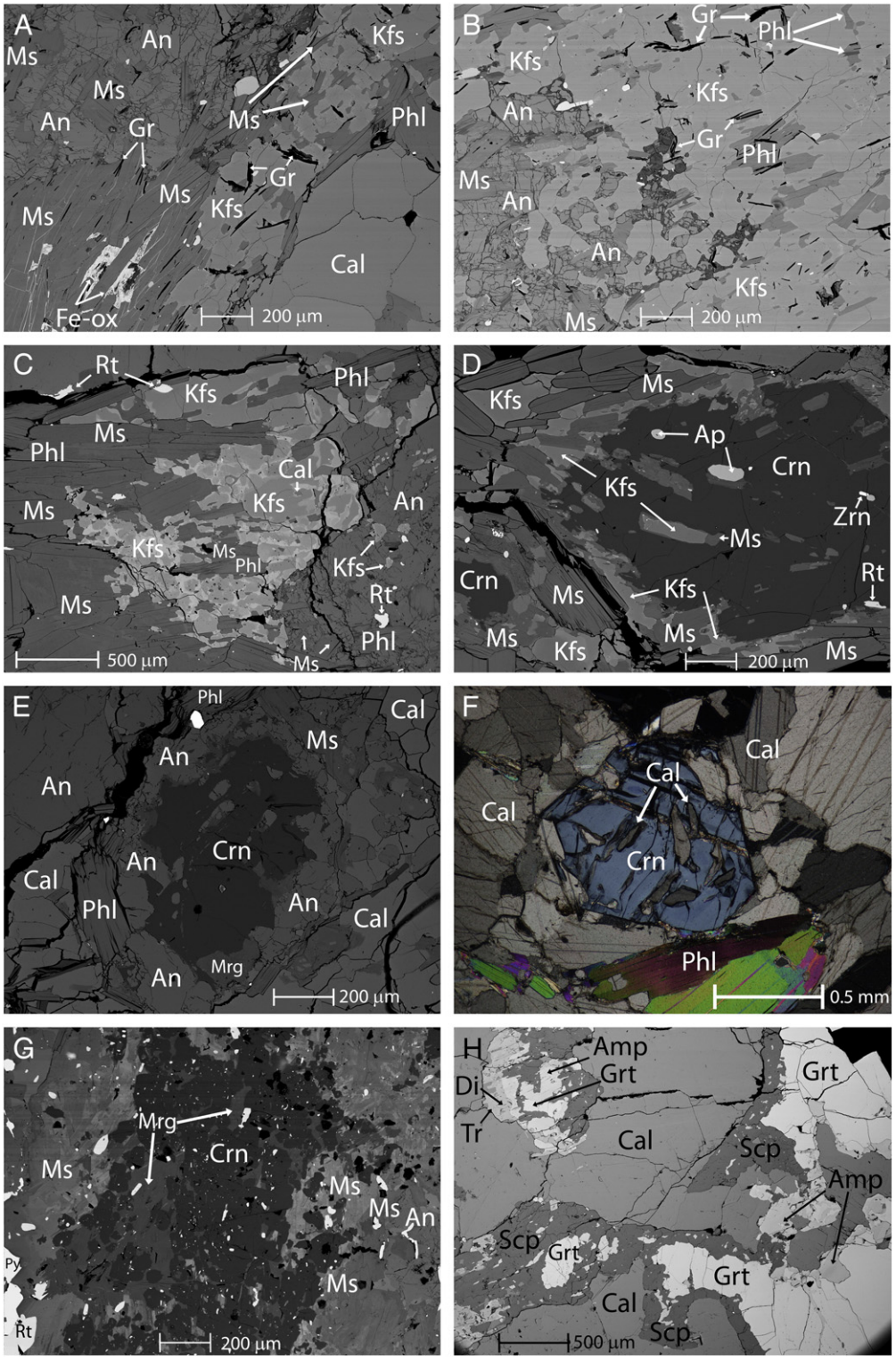

Fig. 4. Optical microphotograph and BSE images of mineral assemblages in mica-feldspar layers and garnet in marble. A) BSE image of replacement of muscovite by anorthite and K-feldspar. Note corroded rims of muscovite relicts in anorthite and phlogopite and muscovite in K-feldspar. B) BSE image of corroded grains of muscovite and phlogopite in anorthite and K-feldspar. Note the intergrowth of anorthite and K-feldspar as well as relicts of muscovite in anorthite and phlogopite in K-feldspar. C) BSE image of Ba-rich K-feldspar replacing muscovite and anorthite. The light areas in the K-feldspar and muscovite are enriched in Ba. D) BSE image of corundum enclosed in muscovite and K-feldspar, with inclusions of apatite, zircon, muscovite, K-feldspar, and rutile. E) BSE image of corundum with anorthite inclusions surrounded by anorthite, phlogopite, and calcite, altered to margarite (Mrg). F) CPL optical microscope image of Type 2 euhedral corundum with calcite inclusions within marble. G) BSE image of Type 3 fine-grained corundum with alteration to margarite and Ba-enriched muscovite within plagioclase. H) BSE image of scapolite and Na,K-amphibole (Amp) coronas around garnet. Diopside is replaced by tremolite.
Mineral name abbreviations are after Whitney and Evans (2010).

inclusions of calcite, and if the inclusions are abundant, they give the crystals a skeletal appearance. The fine-grained type (3) grain size is generally less than 1 mm. The aggregates are usually rather small (<1 cm), sometimes intergrown with Ba-rich K-feldspar or anorthite, overgrown by phlogopite and can be strongly altered. All of the corundum types seem to have non-preferred orientations.

In some instances euhedral crystals of scapolite replace anorthite; they can enclose common muscovite. Corundum associated with anorthite, scapolite and K-feldspar was replaced by margarite or Ba-enriched muscovite where it was accessible to late fluids (Fig. 4G).

5.1.2. Diopside–tremolite laminations

Laminations with common fibrous tremolite replacing euhedral crystals of diopside occur sporadically throughout the marble unit. The laminations are occasionally folded and vary in grain size and thickness; euhedral diopside crystals can be up to 8 cm long (typically 2–4 cm), and the thickness ranges between 1 and 15 cm. The pseudomorphed diopside grains contain tremolite with very small quartz and calcite blebs. Graphite laminations sometimes intersect the diopside-bearing layers as veinlets along the intergranular spaces between calcite grains; graphite aggregates form around the tremolite pseudomorphs and around diopside relics within them. A rare (prograde) euhedral tremolite + calcite assemblage was found in the marble.

5.1.3. Minor assemblages in the marble

A single sample of dark gray spinel crystals rimming pink corundum crystals was found in marble debris near the outcrop localities. Spinel was confirmed by X-ray diffraction.

The assemblage diopside–garnet–Na,K-amphibole–scapolite was found close to a rare quartz lens in the marble. Garnet and diopside are primary minerals in the assemblage. The garnet is rimmed by coronas of scapolite and Na,K-amphibole. The Na,K-amphibole appears to replace diopside when in contact with garnet and scapolite (Fig. 4H), otherwise the diopside is replaced by tremolite.

A single sample of a fine-grained aggregate of brown tourmaline was found in a medium-grained calcite layer. The tourmaline rarely forms euhedral crystals up to 5 mm in calcite pockets.

5.1.4. Non-siliceous laminations

Graphite laminations are common throughout the marble as irregular veinlets. In most cases they appear to post-date the metamorphic assemblages. Rare sheared magnetite-rich layers occur in the marble. The magnetite is enclosed in calcite with relicts of dolomite.

All types of layers and laminations are locally cut by shear zones (up to 20 cm wide) which extend for several tens of meters on the outcrop surface and vary in grain size and mineral abundance. Very fine-grained, black-gray laminations typically contain graphite, apatite, and pyrite, whereas coarser laminations are gray in color and contain more silicate minerals.

5.2. Gneiss

The gneiss which hosts the marble is strongly foliated, with biotite and feldspathic leucosome layers defining the foliation of the rock. The rock fabric is heterogeneous with (1) K-feldspar- and diopside-rich, (2) plagioclase-rich, and (3) biotite-rich layers. The rock composition varies between calc-gneiss (Kfs + Di and Pl layers) and pelitic gneiss (biotite-rich layers). The contents of Ca-rich minerals vary; with increasing Ca in the rock, diopside, K-feldspar, calcite, and titanite increase in abundance, and biotite, quartz, plagioclase, garnet, and sillimanite (±tourmaline) decrease. Trace amounts of graphite are locally present. All minerals are anhedral with the exception of subhedral diopside and titanite.

6. Mineralogy

6.1. Corundum

Most of the studied corundum is pink to red, but blue, violet and colorless varieties occur as well. The amount of gem-quality material is limited and only a very small percentage can be called ruby or sapphire.

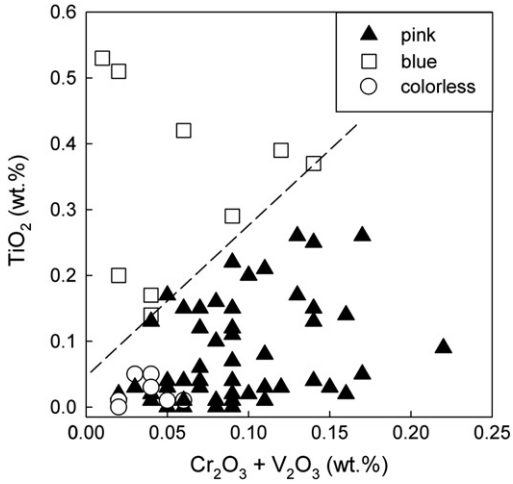

Fig. 5. Trace elements (determined by EMPA) in corundum of different color from the Revelstoke occurrence.

Some crystals have a pink core and blue-violet rim alternating with colorless zones. The pink corundum is characterized by elevated contents of Cr_2O_3 (≤0.21 wt.%) and variable amounts of TiO_2 (≤0.25 wt.%; Fig. 5, Table 1). The blue corundum is enriched in TiO_2 (up to 0.53 wt.%); the Fe_2O_3 content in such grains is generally similar to that in the pink variety, ranging from 0.01 to 0.07 wt.%. Contents of V_2O_3 are low in both varieties (usually <0.03 wt.%). The colorless variety exhibits very low contents of all trace elements (Fig. 5).

6.2. Calcite and dolomite

Calcite is the dominant carbonate mineral in the marble. It contains only trace amounts of MgO (<1.1 wt.%), MnO (<0.63 wt.%), and FeO (<1.8 wt.%). There is a slight enrichment in Mn and Fe near the contact with the gneiss. There is also a slight enrichment in Fe near the contact of mica-feldspar layers with the marble. The trace Mg contents appear to vary randomly within the marble body. Dolomite was identified in a single sample by powder XRD, but was not analyzed by EPMA. Dolomite was also identified as small relict crystals within calcite in a magnetite-rich layer in the marble.

6.3. Mg,Fe-micas

Phlogopite from the float locality was observed in two textural and compositional varieties. The most common phlogopite type occurs in silicate layers, either in the calcite matrix or rimming muscovite aggregates. It has high Al contents (~1.9 apfu), and low contents of the trace elements (0.06–0.10 apfu Ti; <0.03 apfu V; 0.00–0.01 apfu Cr). Rare phlogopite that occurs as inclusions within calcite grains in the carbonate matrix has elevated contents of Ti (0.10–0.12 apfu), V (0.05–0.08 apfu), and Cr (0.01–0.02 apfu). Both phlogopite varieties contain low contents of F (0.05–0.20 apfu), Na (<0.03 apfu) and Ba (<0.05 apfu). In rocks from both outcrop locations, phlogopite was observed as inclusions in anorthite (aggregates with Ba-rich K-feldspar ± corundum); it has significantly elevated contents of Fe (0.25–0.35 apfu) compared to the normal values for phlogopite in samples from the float (Appendix A and C, Suppl. Fig. A2, Suppl. Table C1). Several trace elements in phlogopite (e.g., F, Ca, and Ti) are on average slightly higher in samples from outcrop locations.

The phlogopite observed in the marble represents a solid solution between major phlogopite (42–77%) and eastonite (42–10%), minor muscovite and low amounts of oxy-phlogopite and kinoshitalite/ganterite components. Although Ba could substitute for K and Ti for Mg in the phlogopite structure as a kinoshitalite component, their high ratio and negative correlation of Ti and Mg suggest that

they enter the mica independently by the substitutions $BaAl(KSi)_{-1}$ (phlogopite/muscovite–kinoshitalite/ganterite) and $(Ti\square)Mg_{-2}$ (phlogopite–oxy-phlogopite). Barium-rich phlogopite is a common accessory mineral in marbles or schists associated with metavolcanics (Bol et al., 1989) or with base metal and barite hydrothermal deposits (e.g., Doležalová et al., 2006; Pan and Fleet, 1991).

Biotite from the host gneisses have a significantly higher Fe/Mg ratio, lower amounts of $^{[6]}Al$ and elevated contents of Ti (<0.29 apfu) compared to micas from the marble. Micas from diopside-rich layers contain higher amounts of $^{[4]}Al$ than those in the biotite-rich layers. Host rock micas are a solid solution between major annite and phlogopite, and minor eastonite and siderophyllite. The major substitutions are $Al_2(Mg,Fe)_{-1}Si_{-1}$ (to eastonite/siderophyllite), $Al_2\square(Mg,Fe)_{-3}$ (muscovite) and $FeMg_{-1}$.

6.4. Muscovite and margarite

Muscovite in the marble contains elevated contents of Mg (≤0.30 apfu) and Ti (≤0.09 apfu); contents of Na, Fe, and Ba, are low (Suppl. Fig. A3, Suppl. Table C1). The main chromophores responsible for the green color in micas (V and Cr) are present in trace amounts only; the green muscovite contains 0.00–0.29 wt.% V_2O_3 (0.09 wt.% avg; <0.02 apfu) and 0.00–0.23 wt.% Cr_2O_3 (0.07 wt.% avg.; <0.01 apfu). While contents of V^{3+} increase with Ti, Cr^{3+} does not show a similar trend in most samples, although its ionic radius is more similar to that of Ti^{4+} in octahedral coordination (Shannon, 1976). The composition of some of the muscovite from the outcrop localities is enriched in Fe + Mg and Ba (Suppl. Fig. A3). The slightly increased sum of tetrahedral and octahedral cations is due to a solid solution with both aluminoceladonite and trioctahedral micas (biotite, kinoshitalite). The enrichment is related to patchy zoning in muscovite inclusions in K-feldspar replacing the muscovite aggregates.

Fine-grained margarite locally replaces corundum crystals along fractures and rims. Its composition is $(Ca_{0.82}Na_{0.11}K_{0.07})Al_{3.84}Si_{2.16}O_{10}(OH)_2$, suggesting minor paragonite and muscovite components. The high Na content is in agreement with its retrograde origin along with scapolite and rare albite as secondary phases.

6.5. Feldspars

The prevailing feldspar in the mica-feldspar layers is plagioclase. Its composition ranges from $An_{0.85}$ to $An_{1.00}$, but most of the data fall in the range from $An_{0.90}$ to $An_{0.98}$. The outcrop samples are less variable (An_{89}–An_{97}). Contents of trace elements (K, Fe, Ba) are below their detection limits.

The compositional data for K-feldspar in the mica-feldspar zones show low amounts of Na (Ab_{3-10}) and elevated contents of Ba, ranging from ~0.02 to 0.16 apfu (Suppl. Fig. A4), falling in the field of hyalophane (Deer et al., 2001). The highest Ba and Na-contents were found in anhedral grains of finely zoned K-feldspar around muscovite aggregates (especially from the outcrops) where it forms at the expense of Ba-bearing muscovite.

6.6. Scapolite

Scapolite from mica-feldspar layers exhibits narrow compositional variability in meionite–marialite components ranging in X_{Ca} [Ca / (Ca +Na + K)] from ~0.66 to 0.80, except for two isolated analytical spots from crystal terminations in a carbonate pocket that have X_{Ca} ~0.48 (Fig. 6, Suppl. Table C2). The Cl contents between 0.05 and 0.27 apfu are lower than expected for ideal marialite–meionite solid solution due to a significant mizzonite component (Na-bearing, Cl-free meionite) introduced in the scapolite structure by the substitution $(NaSi)(Ca_{-1}Al_{-1})$. Low amounts of K (0.05–0.32 apfu) are positively correlated with Na and Cl contents. Rare scapolite in coronas around garnet in marble have high amounts of the marialite component (<0.5 apfu Cl, <2.17 apfu Na + K)

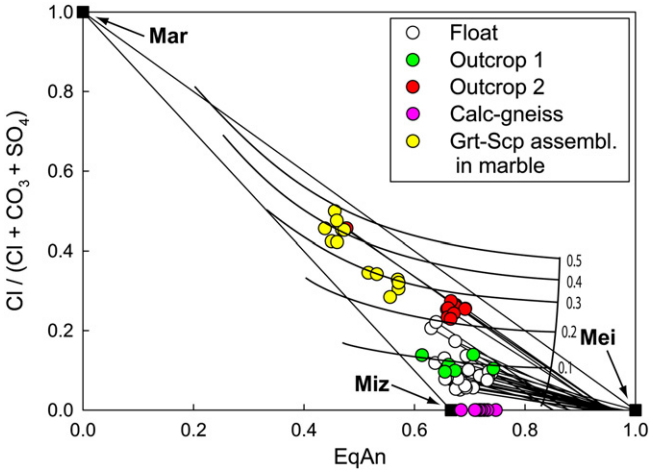

Fig. 6. Compositional diagram for scapolite showing the meionite, marialite, and mizzonite solid solutions in terms of Cl / (Cl + CO_3 + SO_4) and equivalent anorthite EqAn = (Al − 3) / 3.
The curves indicate NaCl content of fluids according to the experimental data of Ellis (1978) for 4 kbar and 750 °C.

comparable to the extreme values from mica-feldspar layers. Scapolite from the host rocks is compositionally distinct; it is Cl-free and contains significant mizzonite with X_{Ca} = 0.81–0.84 only (Fig. 6).

The anorthite associated with scapolite has a wide compositional range of $An_{0.85}$–$An_{1.00}$. The scapolite which originated by anorthite replacement has higher Na contents, which is expressed by lower equivalent anorthite values (0.47–0.74). This feature was also observed in secondary scapolite after anorthite at other localities (Kullerud and Erambert, 1999; Markl and Piazolo, 1998; Pan et al., 1994). The elevated albite component in plagioclase associated with steeper tie-lines in Fig. 6 indicates partial reequilibration of plagioclase with late Na,Cl-enriched fluids at the end of scapolite crystallization.

6.7. Pyroxene

The pyroxene in the marble is pure diopside with negligible amounts of Na, Al, and Fe. In the garnet–scapolite assemblage, the pyroxene is compositionally zoned with X_{Mg} [X_{Mg} = Mg / (Mg + Fe)] ranging from 0.53 to 0.65.

Clinopyroxene in the calc-gneiss exhibits compositional zoning with X_{Mg} = 0.64–0.71 in the crystal cores and X_{Mg} = 0.47–0.58 on their rims. Elevated contents of Al_2O_3 up to 1.81 wt.% and Na_2O up to 0.25 wt.% were locally found in crystal cores, most likely representing non-equilibrated remnants of the peak metamorphic assemblage.

6.8. Garnet

Rare garnet found in marble ($Alm_{48-67}Grs_{21-35}Sps_{6-11}Prp_{5-10}$) is compositionally similar to the garnet that occurs in the gneisses. In the pelitic gneiss the garnet is Ca-poor and falls within the compositional range of $Alm_{66-69}Grs_{17-21}Sps_1Prp_{9-16}$ with slightly elevated Mg and Ca in the rims; in the calc-gneiss the garnet is enriched in Ca with composition $Alm_{31-40}Grs_{52-53}Sps_{2-4}Prp_{5-14}$.

6.9. Amphiboles

Amphibole that replaces diopside within the marble is tremolite containing minor ^{T}Al and Na (tschermakite and edenite components; Suppl. Fig. A5, Suppl. Table C3); nomenclature after Leake et al., 2004. In the garnet assemblage in the marble, the amphibole has a lower Mg/Fe ratio, higher contents of Al and Fe^{3+}, and the composition ranges from ferro-actinolite and actinolite to ferrohornblende, with very low amounts of Na + K (Suppl. Fig. A5b). However, amphiboles replacing

garnet in the same assemblage are mainly potassic-ferropargasite and minor hastingsite; they are rich in Na + K (>0.5 apfu) and Al + Fe^{3+} (>1.5 apfu), and have Mg > Fe^{2+}. The major chemical changes in the amphiboles can be expressed by a combination of edenite ($Na^{T}Al\square_{-1}Si_{-1}$) and tschermakite ($Al^{T}AlR^{2+}_{-1}Si_{-1}$) substitutions (Suppl. Fig. A5c). Most of the data show an ideal trend with a 1:1 ratio towards hastingsite/pargasite as a substitution $(Na,K)(Al,Fe^{3+})^{T}_{1}Al_2\square_{-1}(Mg,Fe^{2+})_{-1}Si_{-2}$. However, data lying out of the ideal trend, and those with Si < 6 apfu indicate minor substitution $(Na,K)(Al,Fe^{3+})^{T}_{2}Al_3\square_{-1}(Mg,Fe^{2+})_{-2}Si_{-3}$ (1:2 ratio of edenite:tschermakite substitutions) towards sadangaite as well.

At the contact between the marble and gneiss, ferro-actinolite occurs as a breakdown product of rare hedenbergite (ca. $Hdn_{60}Di_{40}$), whereas scarce associated fayalite ($Fa_{87}Fo_{10}Tep_3$) is replaced by grunerite or ferro-anthophyllite (Suppl. Fig. A5a). Both substitution schemes observed in tremolite apply to a lesser extent in ferro-actinolite (Al + Fe^{3+} ≤ 0.18 apfu) and grunerite (Al + Fe^{3+} ≤ 0.14) as well; contents of Na are lower than 0.04 apfu in both amphiboles.

6.10. Other accessory minerals

Apatite is the most common accessory phase. It contains low concentrations of the usual minor cations like Mg, Mn, Fe, and Sr (<0.004 apfu; Suppl. Table C4). It is always F-dominant (0.63–0.79 apfu) with elevated Cl (0.07–0.17 apfu) and OH (0.08–0.23) contents. Rarely, compositions with 0.51 apfu F, 0.13 apfu Cl, and 0.36 apfu OH were observed. The elevated chlorine content is in contrast to pure fluorapatite reported from the nearby Mount Grace carbonatite (Höy, 1987).

Rutile in the mica-feldspar layers contains elevated contents of V_2O_3 (<0.64 wt.%) and Nb_2O_5 (<1.24 wt.%), and trace amounts of CaO (<0.38 wt.%), Cr_2O_3 (<0.18 wt.%), and FeO (<0.12. wt.%; Suppl. Table C5). Rutile from the host gneisses is V-free and contains trace amounts of Cr_2O_3 (<0.22 wt.%), FeO (<0.47 wt.%), and Nb_2O_5 (<0.35 wt.%). Elevated V_2O_3 (up to 5.39 wt.%) and Nb_2O_5 (up to 0.9 wt.%) are commonly reported from graphite-rich metasedimentary rocks worldwide (e.g., Canet et al., 2003; Houzar and Cempírek, 2011).

Titanite in the marble and host gneisses have similar chemical compositions (Suppl. Table C6). They exhibit significant $(Al,Fe^{3+})(OH,F)(TiO)_{-1}$ substitution with up to 0.14 apfu F, 0.11 apfu OH, 0.14 apfu Al, and 0.03 apfu Fe^{3+}, commonly with (Al + Fe) ≫ F. Other substitutions (such as those involving e.g. V, Cr, Zr, Nb, Sn; Cempírek et al., 2008) usually observed in titanite are below detection limits. The substitution of Al and OH in titanite is typical in high pressure metamorphic rocks (e.g., Harlov et al., 2006; Tropper et al., 2002) whereas Al,F-rich titanite is typical in low-pressure calc-silicate rocks (e.g., Cempírek et al., 2008; Markl and Piazolo, 1999).

Rare tourmaline (Suppl. Table C7) from the marble is F-, Ca-, O-rich dravite (X_{Mg} = 0.97–0.98; F ≤ 0.30 apfu, Ca ≤ 0.36 apfu, ^{W}O ≤ 0.39 apfu). A single spot representing fluor-dravite (0.47 apfu F) was observed. It differs from the tourmaline in the host gneisses, which contains cores of Fe-rich dravite (X_{Mg} = 0.60–0.75, F ≤ 0.35 apfu, Ca ≤ 0.35 apfu, ^{W}O ≤ 0.46 apfu) and Ca,Fe-enriched rims of schorl-dravite, Na-rich uvite and fluor-uvite (X_{Mg} = 0.46–0.75, 0.34–0.61 apfu Ca) with Al and ^{W}O contents lower than the cores. The tourmaline in marble has higher contents of V (0.012–0.025 apfu) than the tourmaline in gneiss (≤0.010 apfu); contents of Cr are similar (≤0.016 apfu). The Cr and V contents are very low compared to the tourmaline formed in Cr,V-rich metasediments (for review see Cempírek et al., 2013). Members of the dravite–uvite solid solution with variable contents of F and elevated ^{W}O are common in metacarbonates with an evaporite component (e.g., Bačík et al., 2012; Garnier et al., 2008).

7. Whole-rock geochemistry

Marble, calc-silicate within marble, and the gneisses were analyzed for major and trace elements in order to determine possible sources of trace elements in corundum (Al, Ti, V, Cr, Fe) and their relative mobilities (Table 2). Fig. 7 shows major and trace elements of analyzed samples compared to Al_2O_3 which is considered one of the least mobile elements in skarn systems (Meinert et al., 2005) and represents the aluminosilicate components in each rock. Contents of the main immobile elements (Ti, V, and Cr) in the marble and host rocks positively correlate within a narrow range with Al_2O_3 suggesting the same homogenous source of the gneiss and mica-feldspar layers and their formation by mechanical mixing of the two lithologies. Contents of SiO_2 and FeO are strongly depleted in the mica-feldspar layers compared to the mechanical mixing line between marble and gneiss (Fig. 7) whereas K_2O and CaO in the mica-feldspar layers fit within the mechanical mixing range. Contents of MgO are variable in agreement with their higher mobility and original heterogeneity within the marble. Calc-gneiss samples have lower contents of major elements (except for V) compared to the pelitic gneiss samples. In the mica feldspar layers, the contents of U are sometimes higher than in the host rock whereas Th correlates positively with Al_2O_3 (Fig. 7). The contents of V correlate well with the aluminosilicate component content and also with Ti, Cr, Co, and Ni (Fig. 8). The correlation of V and Ti can be also observed in data from metapelitic rocks and amphibolites in Units 6a and 6b (Höy, 2001).

The REE patterns in the gneiss are characterized by elevated REE-contents (~244 ppm), enrichment in LREE (La_{CN}/Lu_{CN} ~ 15.5), and distinct negative Eu-anomaly (Eu/Eu* ~ 0.55; Fig. 9). The marble REE values are close to their detection limits (0.11–1.66 ppm) but their patterns are generally enriched in LREE. The carbonate layers between mica-feldspar layers are enriched in REE (8.15–15.09 ppm) compared to the pure marble. They are enriched in LREE (La_{CN}/Lu_{CN} ~ 8.3–18.2) and exhibit a positive Eu anomaly (Eu/Eu* 1.53–2.86). The mica-feldspar layers are compositionally heterogeneous and the REE contents vary between 5.48 and 165.15 ppm (Fig. 9). All samples are enriched in LREE (La_{CN}/Lu_{CN} ~ 6.4–23.7). The Eu anomaly is most pronounced and negative in REE- and silicate-rich samples (Eu/Eu* ~ 0.3) and it gradually increases to positive values in more carbonate-rich samples (Eu/Eu* 0.5–1.27). Contents of Y generally positively correlate with Dy and Ho, and with REE (Table 2).

8. ^{40}Ar–^{39}Ar dating of micas

Phlogopite and muscovite from mica-feldspar layers within marble from the float locality were dated using the ^{40}Ar–^{39}Ar method in order to help constrain the thermal history of the study area. Both micas provided similar ages of 47.32 (±0.29) Ma and 47.10 (±0.26) Ma, respectively. Closure temperatures of phlogopite and muscovite are ~500 and 529 °C (for a cooling gradient of 100 °C/Ma; Baxter, 2010), so both ages are interpreted to represent the late cooling stage of the marble.

Crowley and Parrish (1999) and Crowley et al. (2001) summarized and provided new age data for the Monashee Complex and reconstructed the uplift history of units below the Monashee décollement. Using zircon and monazite U–Pb data, they identified the thermal peak conditions of the Frenchman Cap dome rocks around 58 Ma. Subsequent isothermal decompression was followed by fast isobaric cooling starting from ~51 Ma in the Monashee cover sequence (Crowley and Parrish, 1999). The rate of the uplift was estimated by Sanborn (1996) using hornblende and biotite Ar–Ar ages. Our phlogopite and muscovite ages are ~1 Ma younger than those reported by Sanborn (1996) for biotite and confirm the fast uplift rate in the Frenchman Cap dome.

9. Stable isotopes

Carbonate $\delta^{18}O$ values for marble (13.4–17.5‰), mica-feldspar layers within marble (13.5–16.6‰), and host gneiss (14.8–15.4‰) at the Revelstoke occurrence are variable (Fig. 10A). An anomalously low $\delta^{18}O$ value was recorded in a magnetite-bearing marble sample (12.1‰). Most of the values of $\delta^{13}C$ in the calcite marble are between ~0 and −1.2‰ with several lower values down to −2.9‰ in samples

Table 2
Whole-rock geochemistry.

	G069AM	G014MU	G046X	G014CSU	G023CSD	G023CSU	G063BCSM	G069BCS	G071P	G070P	G055P	G058P
	Marble			Mica-feldspar layers in marble					Calc-gneiss		Pelitic gneiss	
P_2O_5 (wt.%)	0.01	<0.01	<0.01	0.17	0.05	0.08	0.03	0.04	0.11	0.16	0.06	0.03
SiO_2	0.17	0.65	1.29	8.20	3.18	7.57	16.35	4.46	47.7	55.5	55.6	55.8
TiO_2	<0.01	0.01	0.01	0.21	0.05	0.13	0.61	0.10	0.64	0.71	0.78	0.77
Al_2O_3	0.03	0.32	0.32	6.43	2.21	6.65	11.60	2.08	15.3	17.15	18.8	18.8
Cr_2O_3	<0.01	<0.01	<0.01	0.01	<0.01	<0.01	0.01	<0.01	0.01	0.01	0.01	0.01
Fe_2O_3	0.54	0.21	1.99	0.66	0.21	0.41	2.18	1.33	5.29	6.74	5.47	7.16
MgO	0.34	0.57	9.48	1.31	1.41	2.32	7.66	4.40	3.31	3.42	2.77	2.92
CaO	55.6	54.3	41.5	44.40	51.80	44.70	29.90	45.80	17.25	8.32	7.17	3.97
MnO	0.03	0.03	0.13	0.03	0.04	0.03	0.05	0.17	0.06	0.09	0.07	0.07
SrO	0.03	0.07	0.08	0.07	0.08	0.08	0.05	0.07	0.08	0.06	0.03	0.05
BaO	0.06	0.01	0.01	0.12	0.02	0.06	0.21	0.09	0.07	0.14	0.41	0.08
Na_2O	0.05	0.05	0.06	0.12	0.07	0.12	0.22	0.14	1.02	0.38	0.57	1.32
K_2O	0.01	0.12	0.14	1.04	0.31	0.80	3.42	0.91	2.29	1.77	4.21	2.84
LOI (%)	43.4	43.9	43.6	35.4	40.4	34.7	24.7	39.2	3.09	0.89	1.2	1.7
Total (%)	100.5	100	98.6	98.2	99.8	97.7	97.0	98.8	96.2	95.3	97.2	95.5
C	12.25	12.1	12.15	9.82	11.15	9.81	6.78	11.55	1.37	0.25	0.32	0.36
S	<0.01	<0.01	<0.01	<0.01	<0.01	<0.01	0.26	<0.01	0.27	0.33	0.36	0.31
V (ppm)	7	11	10	66	28	58	91	32	142	110	87	91
Cr	<10	<10	<10	40	<10	30	70	10	90	90	120	100
Co	<1	<1	<1	6	<1	<1	7	<1	13	10	13	12
Ni	<1	<1	<1	25	<1	3	23	4	30	26	33	40
Cu	<1	<1	<1	3	<1	1	18	<1	27	30	31	34
Zn	5	15	82	44	11	20	387	61	105	109	45	132
Ga	<0.1	0.3	0.4	9.3	2.5	6.4	19.8	1.8	24.2	26.9	28.2	28.3
As	<0.1	<0.1	<0.1	0.1	<0.1	<0.1	<0.1	<0.1	<0.1	<0.1	<0.1	<0.1
Se	0.2	0.2	0.3	0.3	0.2	0.2	0.9	0.2	0.5	0.5	0.6	0.4
Rb	0.2	2.6	6.5	39.7	15.7	31.7	143	42.3	120	125	179.5	150
Sr	287	584	654	581	641	632	414	564	755	519	292	397
Y	<0.5	3.5	2.6	4.7	2	2.3	6.3	1.1	24.1	28.6	27.3	24.7
Zr	<2	15	9	41	17	22	86	13	121	183	127	114
Nb	<0.2	0.3	0.2	5.7	1.6	3.7	11.6	1.4	16.9	36.1	22.4	18.3
Mo	<1	<1	<1	<1	<1	16	3	23	<1	<1	<1	<1
Ag	<0.5	<0.5	<0.5	<0.5	<0.5	<0.5	1.2	<0.5	<0.5	<0.5	<0.5	<0.5
Cd	<0.5	<0.5	<0.5	<0.5	<0.5	<0.5	0.9	<0.5	<0.5	<0.5	<0.5	<0.5
Sn	<1	<1	<1	1	<1	<1	2	<1	2	3	3	3
Sb	0.05	<0.05	<0.05	0.06	0.06	0.06	2.17	0.15	<0.05	<0.05	<0.05	<0.05
Te	0.01	0.03	0.02	0.02	0.02	0.01	0.02	0.03	0.01	0.01	0.01	0.01
Cs	0.02	0.07	0.44	0.72	0.6	1.3	5.25	1.85	4.77	6.49	4.85	5.63
Ba	9.7	59.4	76.6	1065	259	535	1705	831	678	1080	3430	710
La	<0.5	3.1	1.6	5.8	3.9	4.2	33.2	1.2	51.2	63.9	57.4	57.1
Ce	<0.5	5.5	3.7	9.9	6.2	6.7	56.3	2	89.9	114	102	100.5
Pr	0.04	0.72	0.59	1.22	0.79	0.85	6.08	0.26	11.15	14.2	11.75	12.7
Nd	0.2	2.9	2.8	4.5	2.9	3.2	17.3	1.1	39.3	49.4	43.9	44.6
Sm	0.03	0.63	0.7	0.96	0.51	0.59	1.84	0.21	6.63	8.35	7.49	7.45
Eu	<0.03	0.32	0.52	0.31	0.08	0.09	0.19	0.04	1.2	1.39	1.25	1.31
Gd	<0.05	0.64	0.57	0.93	0.45	0.49	2.17	0.17	5.96	7.47	6.71	6.61
Tb	<0.01	0.08	0.08	0.13	0.06	0.07	0.22	0.03	0.77	0.99	0.96	0.88
Dy	<0.05	0.49	0.39	0.73	0.31	0.35	1.19	0.14	4.21	5.37	4.93	4.68
Ho	<0.01	0.1	0.07	0.15	0.06	0.07	0.26	0.03	0.83	1.06	0.94	0.92
Er	<0.03	0.29	0.18	0.46	0.2	0.23	0.88	0.12	2.55	3.12	2.94	2.84
Tm	<0.01	0.04	0.03	0.07	0.03	0.03	0.13	0.02	0.36	0.43	0.42	0.4
Yb	<0.03	0.24	0.17	0.49	0.18	0.22	0.99	0.14	2.28	2.84	2.71	2.51
Lu	<0.01	0.04	0.02	0.07	0.03	0.04	0.17	0.02	0.36	0.42	0.43	0.38
Hf	<0.2	0.4	0.3	1.2	0.5	0.8	2.7	0.4	3.5	5.1	4.3	3.4
Ta	<0.1	<0.1	<0.1	0.4	0.1	0.2	0.9	0.1	1.2	2.3	1.6	1.3
W	1	1	1	1	1	1	2	1	2	2	2	2
Hg	0.012	0.008	0.013	0.012	0.013	0.009	0.012	0.012	<0.005	<0.005	0.009	0.007
Tl	<0.5	<0.5	<0.5	<0.5	0.5	0.6	0.7	<0.5	0.8	0.7	1.2	0.7
Pb	6	19	28	12	7	6	758	19	19	12	21	19
Bi	<0.01	0.11	<0.01	0.03	0.01	0.01	0.73	0.04	0.14	0.24	0.13	0.22
Th	<0.05	0.45	0.41	7.33	0.91	1.95	7.82	0.37	15.55	18.45	17.35	17.8
U	0.57	0.54	1.59	14.45	4.39	9.37	4.69	2.05	3.47	3.12	2.86	2.84
La_{CN}/Lu_{CN}		8.3	8.6	8.9	13.9	11.3	20.9	6.4	15.2	16.3	14.3	16.1
Eu/Eu*		1.53	2.44	0.99	0.50	0.50	0.29	0.63	0.57	0.53	0.53	0.56

with minor fluid alteration or close proximity to mica-feldspar layers; dolomite-bearing calcite marble has a low $\delta^{13}C$ value of −2.8‰. Most $\delta^{13}C$ carbonate values from mica-feldspar layers range between −3.1 and −1.1‰ and are generally lower than carbonate from marble. The lowest $\delta^{13}C$ values were found in the garnet–scapolite rock (−3.2‰) and host calc-gneiss (−4.48 to −2.55‰). The $\delta^{13}C$ values generally decrease in the direction from the marble to mica-feldspar layers (Fig. 10A). Whole rock $\delta^{18}O$ silicate values for mica-feldspar layers within marble (11.1–16.2‰) and gneiss (14.4–15.8‰) at the Revelstoke occurrence are generally high compared to average pelite, but fall

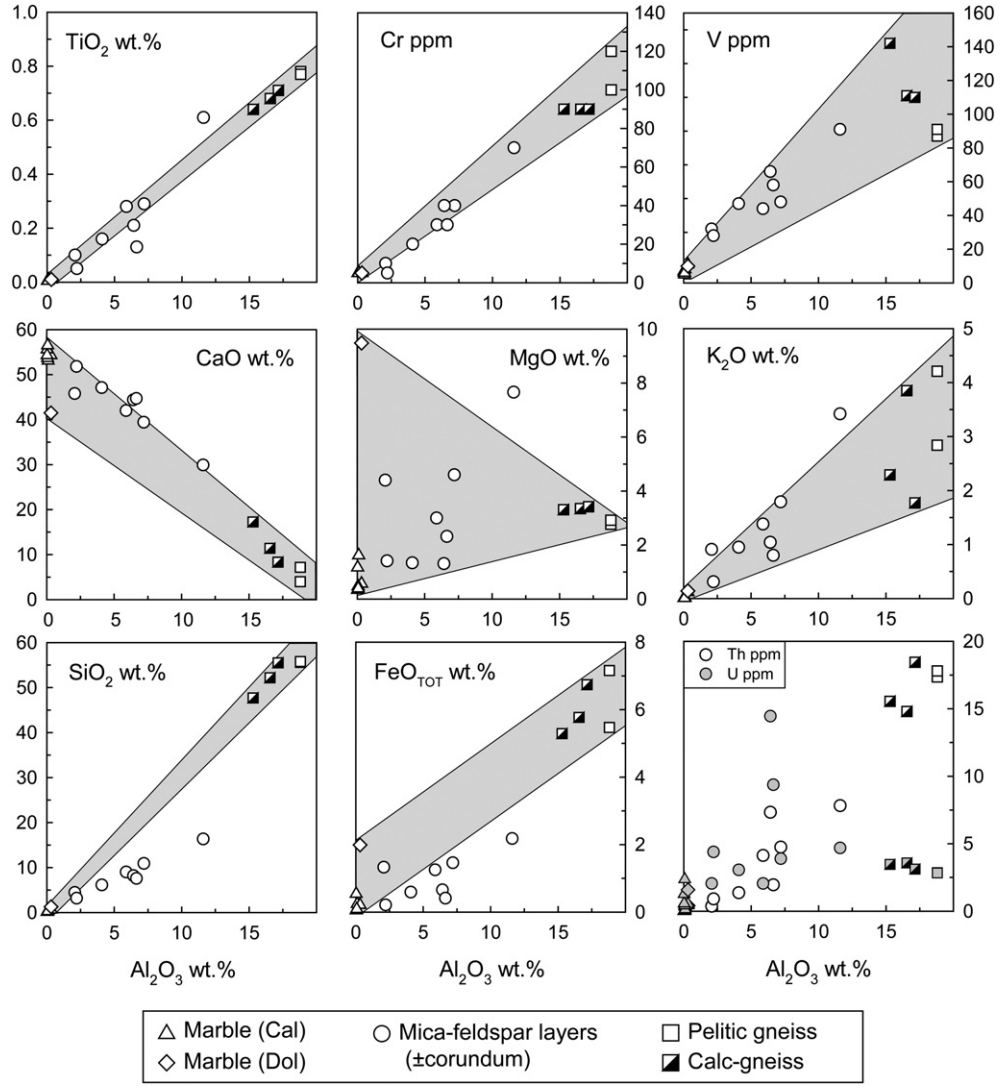

Fig. 7. Contents of immobile trace elements (Ti, Cr, V), selected mobile major elements (Si, Fe), and partially mobile elements (Ca, Mg, K, U, Th) in different lithologies. The compositional space between dolomite marble, calcite marble and gneiss is marked in gray.

within the data range from metasediments in the Monashee Complex and in other units of the Selkirk Allochthon (Figs. 10B, 11). Isolated grains of corundum in calcite have $\delta^{18}O$ values of 10.7 and 11.1‰.

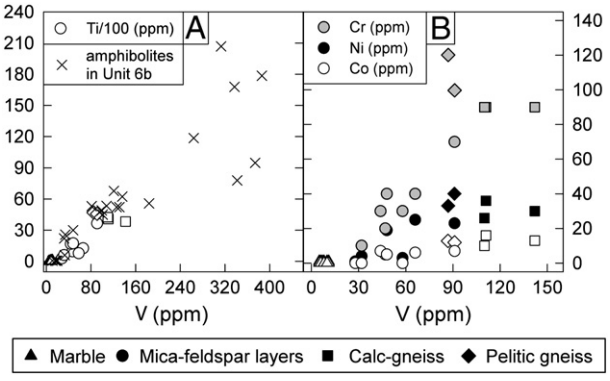

Fig. 8. Geochemistry of selected trace elements in the host rock and marble. Data for amphibolites in Unit 6b are from Höy (2001).

10. Fluid inclusions

Two-phase liquid CO_2-vapor (LCO_2-V) primary fluid inclusions occur within color zones of corundum at the Revelstoke occurrence. The inclusions are ~30 μm to 144 μm in size and include concave, rectangular, elongate and irregular shapes. The CO_2 vapor at room temperature occupies ~4% of the inclusion volume. The composition of fluid inclusions within corundum was determined by microthermometry (Table 3). After rapid cooling of the sample to −190 °C, slow warming caused phase changes from solid to liquid to vapor; i.e., melting of CO_2 ice (−93.5 to −73 °C), CO_2 solid (−58.2 to −56.6 °C), and homogenization of CO_2-liquid-vapor (24.7–27.2 °C; Table 3). Melting temperatures below the triple point for CO_2 (−56.6 °C) indicate the presence of minor CH_4 and/or N_2 (Van den Kerkhof and Thiéry, 2001).

Fluid inclusions in corundum from a variety of different protoliths typically have irregular or negative shapes and commonly contain nearly pure CO_2 fluids (Giuliani et al., 2003). Other fluids in addition to CO_2 that can occur within corundum fluid inclusions are H_2O, H_2S, N_2, and COS (Giuliani et al., 2003; Limtrakun et al., 2001; Takayuki et al., 2001). Solids are uncommon in corundum fluid inclusions, however, crush leach analysis of fluid inclusions in corundum within marble has revealed the presence of Na, Cl, K, NO_3, and SO_4 at the ppb level (Giuliani et al., 2003). Laser Raman analysis is commonly used to detect

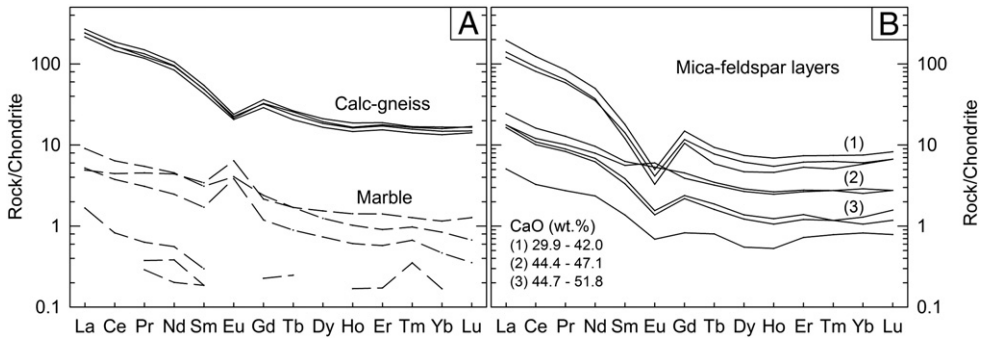

Fig. 9. Chondrite-normalized (Sun and McDonough, 1989) REE-plots for (A) gneiss and marble, and (B) mica-feldspar layers in the marble.

other liquid species in corundum fluid inclusions, but use of this technique was not possible for the Revelstoke corundum due to its high fluorescence under the laser beam.

11. Discussion

11.1. Protolith of silicate assemblages in the marble

The whole-rock geochemical data show that the silicate-rich part of the marble has the same or similar protolith as the host gneisses. Ratios of immobile elements suggest that the two lithologies were mechanically mixed without change in the ratio of aluminosilicates and the main Ti-,V-, Cr-bearing minerals i.e., rutile and titanite (Fig. 8). The mixing could be between the carbonate sediments and pelite or tectonic emplacement of the gneiss within marble. The thin bedding of the silicate-rich layers in marble can be a result of primary sedimentation or tectonic emplacement, but was likely enhanced due to extreme stretching during deformation; the former is more probable because of the frequency and thin bedding of silicate layers. Depletion in SiO_2 and FeO in mica-feldspar layers suggests that these elements were removed from the original silicate layers mixed within marble. Textural evidence for diffusion, fluid flow and mass exchange typical for reaction zones (skarns) between rocks with contrasting compositions (e.g., Meinert et al., 2005) was not observed, which suggest the process responsible for the desilicification and Fe-depletion took place during the prograde path of metamorphism before the main mineral transformations. Prograde fluid-assisted removal of SiO_2 and FeO from the silicate layers, due to high chemical potential gradients between the silicate layers and the marble, is in agreement with the homogenization of oxygen isotopes in carbonates and silicates observed in the marble, mica-feldspar layers, and host gneiss (Figs. 10 and 11) and with the general chemical mobility trends documented at other localities at the contacts of two contrasting lithologies (e.g., Brady, 1977; Joesten, 1977). The combination of the high chemical potential gradient of SiO_2 between the silicate layers and marble, along with the increasing solubility of SiO_2 with increasing temperatures and the formation of $H_3SiO_4^-$ complexes in aqueous fluids (Seward, 1974; Walther and Woodland, 1993), could cause extensive SiO_2 mobilization and explain the depletion in mica-feldspar layers. Furthermore, the chemical potential (and diffusion) gradients could have been enhanced by the thinning of silicate layers within marble during tectonism because of stretching and folding. The reduced solubility and mobility of K and Na compared to Si could be due to the low salinity of the reacting fluids (Pak et al., 2003).

The low Sr contents and their positive correlation with CaO (Table 2) are consistent with a non-evaporitic origin for the original sediment (Moine et al., 1981), and the compositions of all the rock types correspond to those of shales or marls derived from platform sediments (Garnier et al., 2008; Moine et al., 1981). This is in agreement with the original interpretation of the Revelstoke metasedimentary sequence by Höy (1987). Contents of V, Ti Cr, Co, and Ni show positive correlations (Fig. 8), which could indicate a common source from a mafic protolith (e.g., Grapes and Palmer, 1996). With regard to the local geology and rare presence of minor SEDEX mineralization in contact with the marble and common sulfide minerals within the marble, we also considered the influence of the sedimentary-exhalative protolith (e.g., Canet et al., 2003). The scarce data from the Monashee complex SEDEX

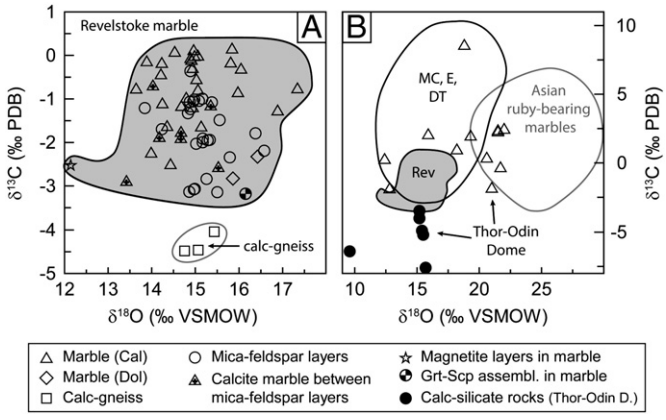

Fig. 10. Coupled $\delta^{13}C$–$\delta^{18}O$ values for carbonates from different lithologies. A) Values for carbonates from the studied lithologies from the Revelstoke occurrence; B) published values for carbonates from other marbles from the Mica Creek (MC), Esplanade Range (E), and Dogtooth Range (DT) ~50 km north of the Monashee Complex in the Selkirk Allochthon (Ghent and O'Neil, 1985), Thor–Odin Dome (Holk and Taylor, 2000) and Asian ruby deposits in marble (Garnier et al., 2008) compared to the studied Revelstoke lithologies ("Rev", dark gray).

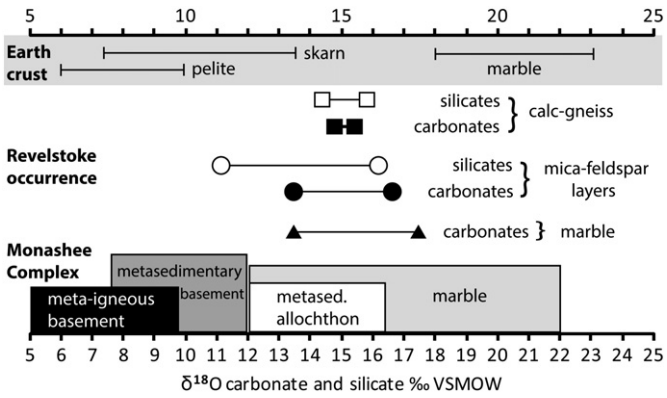

Fig. 11. Range of $\delta^{18}O$ values for carbonate and silicate minerals compared to potential protoliths in the Monashee Complex near the Thor Odin dome (Holk and Taylor, 2000) and to average values for pelites (Hoefs, 2004), skarns (Bowman, 1998), and marbles (Valley, 1986). The plotted carbonates combine both drill-separated and leach-separated samples.

Table 3
Microthermometry results.

($n = 5$)	Max °C	Min °C	Avg °C	σ
Homogenization temperature of CO_2 bubble	23	15	18.2	2.9
Melting temperature of CO_2-ice	−73	−93.5	−82.1	9.0
Melting temperature of CO_2-solid	−56.6	−58.2	−57.5	0.7
Homogenization temperature of CO_2-vapor-liquid	27.2	24.7	25.7	1.0
% CO_2	100	92	94.8	3.5
Molar volume	65.3	61.5	63.0	1.5

mineralization show no correlation of V with Ti, Co, and Ni contents (Höy, 2001), and there is no evidence of significant mixing of the two lithologies. Therefore, the preferred explanation for the elevated Cr and V contents in the marble is the dispersed mafic component (protolith of amphibolites) in the pelitic sediments in Units 6a and 6b and its mixing with the carbonate material before metamorphic overprint.

The variation in REE and Y contents is generally related to the amounts of the silicate component in the individual samples. The LREE enrichment in all patterns is compatible with the presence of accessory apatite, allanite, zircon, and titanite in the gneiss and silicate-rich parts of the marble. The difference in LREE/HREE fractionation in the host gneiss and the most LREE-enriched mica-feldspar layers may be related to the partial melting and remobilization processes in the host gneiss which may have also caused the observed depletion in U due to partial dissolution/alteration of accessory phases (e.g., Rubatto et al., 2008).

The $\delta^{18}O$ and $\delta^{13}C$ values from carbonate vary at the Revelstoke occurrence (Fig. 10A). $\delta^{18}O$ carbonate values for marble (13.5–17.5‰) are lower than expected for normal marble (20–28‰; Valley, 1986), but the $\delta^{13}C$ values (−2.7–0.1‰) are within the normal range for marine carbonates (Hoefs, 2004). The distribution of $\delta^{18}O$ and $\delta^{13}C$ carbonate values follow a generalized devolatization trend (Valley, 1986) where $\delta^{13}C$ is more affected than $\delta^{18}O$. The decrease of $\delta^{13}C$ values in calcite towards the silicate assemblages is likely the result of decarbonation reactions that produce silicates during metamorphism (Fig. 10A; Valley, 1986).

The $\delta^{18}O$ and $\delta^{13}C$ results fall within the range of values observed in marbles from the Mica Creek area and the Thor–Odin dome (Fig. 10B; Ghent and O'Neil, 1985; Holk and Taylor, 2000). The $\delta^{13}C$ values also fall within the range of Asian ruby-bearing marbles, but the $\delta^{18}O$ values are much lower (19.9–28.9‰; Garnier et al., 2008).

The similarity of the $\delta^{18}O$ and $\delta^{13}C$ values of carbonates and the $\delta^{18}O$ values of silicates at the Revelstoke occurrence, Mica Creek area, and Thor–Odin dome likely indicate that sediments at these localities had similar protoliths and/or underwent similar fluid–rock interactions during metamorphism (Valley, 1986). Ghent and O'Neil (1985) attribute the range of $\delta^{18}O$ values at the Mica Creek area to varied protoliths and metamorphic formation conditions whereas the elevated $\delta^{13}C$ values could be attributed to depositional processes prior to metamorphism, such as: (1) Precambrian carbonate-secreting algae, (2) organic material, or (3) travertines. Holk and Taylor (2000) suggest the homogenized $\delta^{18}O$ values in rocks above and less than 200 m below the Monashee décollement at the Thor–Odin dome were caused by the interaction of recycled H_2O-bearing fluids (derived from anatectic and metamorphic processes) and CO_2-fluids (derived from the devolatization of calc-silicate rocks) with the host rocks during the metamorphic evolution of the core complex. These fluids didn't penetrate >200 m into the Monashee Complex because they were channeled along the Monashee décollement. Thick marble units at the Thor–Odin dome are interpreted to be relatively impermeable and retained higher $\delta^{18}O$ values (18–22‰) in contrast to thinner units in leucogranite-rich sections (12.4–15.2‰).

Even though Holk and Taylor (2000) did not see any homogenization of $\delta^{18}O$ values in the Monashee complex between 200 and 400 m below the Monashee décollement, extensive fluid–rock interaction must have affected the Revelstoke rocks which are much deeper (~2 km) below the Monashee décollement because of: (1) the lack of preservation of any normal marine carbonate $\delta^{18}O$ values throughout the entire marble unit (Fig. 10A), (2) similar carbonate $\delta^{18}O$ values in the gneiss and marble (Fig. 10A), and (3) similar silicate $\delta^{18}O$ values in the gneiss and mica-feldspar layers (Fig. 11). The small variation and depletion of $\delta^{18}O$ values of carbonates across the entire marble unit is likely due to variability in the isotopic composition of the original sediments and fluid–rock interactions during metamorphism between carbonate sediments mixed with thin layers of pelitic sediments. Elevated $\delta^{18}O$ silicate values in the host gneiss were also likely influenced by mixing of carbonate and pelitic components or infiltration of late CO_2-rich fluids from the marble. Stretching of pelite layers within the marble during deformation would have decreased their thickness and increased the rate at which exchange could take place between the two lithologies. Recrystallization of carbonate minerals during retrograde metamorphism could also have affected the $\delta^{18}O$ values.

The corundum $\delta^{18}O$ values are much lower than those from worldwide corundum occurrences in marbles, and plot in the skarn field according to Giuliani et al. (2005). However, this classification does not include corundum from mixed pelitic and marble protoliths. The low corundum $\delta^{18}O$ values reflect the $\delta^{18}O$ values of the host marble and mica-feldspar layers.

Previous studies of the Revelstoke occurrence host rocks (Unit 6a, b) by Journeay (1986) and Höy (1987) characterized the unit as a metamorphic equivalent of marls and attributed the presence of scapolite to the salt content of original sediments. Our geochemical and isotopic data support this interpretation and show that mixing of pelitic and carbonate sedimentary material caused elevated Cr and V contents in the marble.

11.2. Chromium and vanadium enrichment

Occurrences of Cr- and V-bearing minerals in marbles, dolomites, and skarns are rather common; they typically occur as a part of metasedimentary sequences containing black shales, SEDEX mineralization, and/or mafic rocks (e.g., Canet et al., 2003; Pan and Fleet, 1991; Treloar, 1987; Uher et al., 2008). Genetically similar Cr- or V-rich assemblages are also commonly found in graphite quartzites and graphite metacherts (e.g., Bačík et al., 2011; Cempírek et al., 2013; Houzar and Cempírek, 2011; Lee and Lee, 2003; Snetsinger, 1966). The common association of high vanadium contents with reduced carbonate rocks is not coincidental. Breit and Wanty (1991) showed mechanisms of vanadium accumulation in carbonaceous rocks with high contents of organically bound sulfur. Vanadium is deposited in sediments under reduced conditions where it is adsorbed to clay minerals; further metamorphic overprint can cause vanadium incorporation in newly formed muscovite and silicates. Geochemical data indicate that the increased amounts of V and Cr most likely originate from the breakdown of mafic rocks. If the V and Cr were released from their original minerals, their retention in reducing conditions could be an important factor in the Revelstoke rocks, which typically contain minor amounts of sulfide minerals and graphite.

Enrichment in V and Cr in the corundum-bearing assemblages is also significantly related to their preferential binding in phlogopite and muscovite. Although minor rutile is enriched in V_2O_3 and Cr_2O_3 ($\leq$0.64 and $\leq$0.18 wt.%), the majority of Ti, V, and Cr in the marble is stored in micas ($\leq$0.09 wt.% V_2O_3 and $\leq$0.23 wt.% Cr_2O_3 in muscovite; $\leq$1.41 wt.% V_2O_3 and $\leq$0.27 wt.% Cr_2O_3 in phlogopite). At the Revelstoke occurrence V and Cr were likely originally bound in silicates and clay minerals, making them available to micas during diagenesis. If V and Cr were originally bound in detrital chromite or rutile, their release would be restricted to high metamorphic temperatures in a H_2O-poor and quartz-free marble system.

11.3. P–T metamorphic path of Frenchman Cap dome

The observed mineral assemblages in metapelites at the Frenchman Cap dome are in agreement with similar rocks at the Thor–Odin dome as described by Hinchey et al. (2006). The P–T path defining assemblages include the prograde reaction biotite + albite + sillimanite + quartz = garnet + K-feldspar + melt (Spear et al., 1999). Journeay (1986) and Höy (1987) identified the clockwise P–T path for the pelitic rocks of the Frenchman Cap dome, with the peak metamorphic assemblages followed by a medium-pressure overprint during unroofing and isobaric cooling.

Calculations of stable equilibrium assemblages from whole rock data were done using the Theriak–Domino software package (de Capitani and Petrakakis, 2010). The assemblage (observed in the studied samples) of garnet + biotite + plagioclase + K-feldspar + kyanite is stable in the range of 700–900 °C and 7.0–12 kbar. The minimum P–T conditions of 720 °C and 8.0 kbar are well constrained by the absence of phengite/muscovite and the presence of kyanite. Ilmenite is not stable in the phengite-free kyanite assemblages; hence, the observed inclusions of ilmenite in garnet are interpreted as relicts of pre-peak prograde metamorphism. During decompression, the retrograde assemblages observed in sillimanite-bearing metapelite of biotite + sillimanite + K-feldspar and biotite + muscovite + plagioclase feldspar became stable between 575 and 700 °C and 4 and 8 kbar. These values generally agree with the P–T path defined by Norlander et al. (2002) and Hinchey et al. (2006). However, the presence of andalusite and cordierite identified by Höy (1987) indicate that the retrograde part of the P–T path took place at lower pressures than was suggested for the Thor–Odin dome by Hinchey et al. (2006).

The assemblage of garnet + biotite on the border of garnet porphyroblasts in biotite-rich layers and the garnet + clinopyroxene assemblage (core compositions) rarely observed in the K-feldspar-rich layers were used for estimation of equilibrium temperatures (Bhattacharya et al., 1992; Krogh, 1988). The calculated temperatures using garnet + biotite and garnet + clinopyroxene thermometers are 675–695 °C and 766–771 °C, respectively. The garnet + biotite temperatures are about 25 °C lower than the lowest values observed by Norlander et al. (2002) in the Thor–Odin dome. The values may be influenced by biotite re-equilibration during retrograde metamorphism and do not represent the peak of metamorphic conditions. On the other hand, the garnet + clinopyroxene temperatures should reflect near-peak metamorphic conditions.

11.4. P–T–X evolution of the marble

Major equilibrium mineral assemblages in the marble are diopside + calcite, phlogopite + calcite, rare tremolite + calcite, and fibrous tremolite + calcite + quartz in the siliceous layers, and magnetite + calcite ± dolomite in the non-siliceous layers. The assemblages of garnet + diopside + scapolite + Na,K-amphiboles are rare. Starting from hydrated dolomitic marble, the first prograde reactions in the marble were:

$$5\ \text{dolomite} + 8\ \text{quartz} + H_2O \rightarrow \text{tremolite} + 3\ \text{calcite} + 7CO_2$$

$$3\ \text{dolomite} + \text{K-feldspar} + H_2O \rightarrow \text{phlogopite} + 3\ \text{calcite} + 3CO_2$$

$$\text{tremolite} + 2\ \text{quartz} + 3\ \text{calcite} \rightarrow 5\ \text{diopside} + 3CO_2 + H_2O.$$

The three reactions took place progressively in a relatively narrow temperature range (Fig. 12a). The occurrence of major diopside + calcite and rare prograde tremolite + calcite assemblages in the marble agrees with the steep P–T path proposed by Hinchey et al. (2006) and with high X_{CO2} in the marble at the pressure peak of metamorphism (Fig. 12a).

Textural relations in the mica-feldspar layers suggest that the mineral assemblage before formation of corundum was muscovite + K-feldspar + anorthite + calcite ± dolomite. Most of the quartz was removed from the system by the following prograde reaction at ~600 °C and ~9 kbar:

$$\text{muscovite} + \text{calcite} + 2\ \text{quartz} \rightarrow \text{K-feldspar} + \text{anorthite} + H_2O + CO_2.$$

Absence of relict kyanite and zoisite in products of the reaction above indicates that the maximum pressure should be ~9 kbar, which is approximately 1 kbar lower than the prograde P–T-evolution at the Thor–Odin Dome (Hinchey et al., 2006).

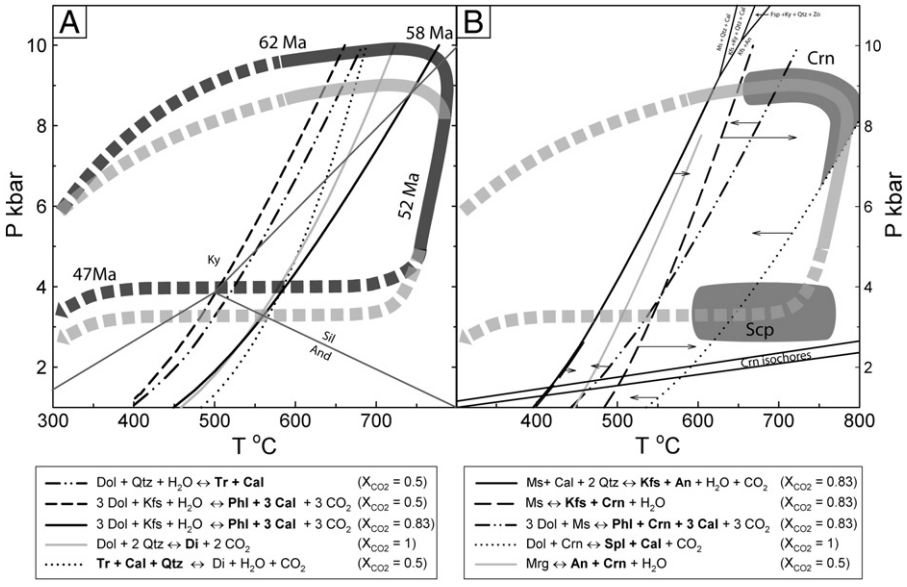

Fig. 12. Major mineral-forming reactions and P–T evolution of the Revelstoke occurrence marble. Bolded mineral names indicate observed mineral assemblages. Arrows indicate position of curves with increasing X_{H2O}. Corundum fluid inclusion isochores are also plotted.

The decarbonation reactions that produced phlogopite and feldspars during prograde metamorphism increased the activity of CO_2 in the system and decreased the reaction temperatures of subsequent reactions promoting the formation of corundum from muscovite in the absence of quartz:

muscovite → corundum + K-feldspar + H_2O

3 dolomite + muscovite → phlogopite + corundum + 3 calcite + $3CO_2$.

At the same P–T-conditions (9 kbar, 700 °C), the last diopside-forming reaction in the marble took place:

dolomite + 2 quartz → diopside + $2CO_2$.

The corundum-forming reactions probably started during prograde metamorphism and high X_{CO2} in the range ~650–700 °C at 8.5–9 kbar (Fig. 12b) and continued during marble decompression. The dry conditions are supported by the pure CO_2 fluid inclusions observed in corundum and by formation of new phlogopite overgrowing muscovite and corundum; the reaction started at the beginning of decompression at ~760 °C and 9 kbar (Fig. 12a). The majority of corundum (types I and II) at the Revelstoke occurrence was produced by the dehydration of muscovite. This is inferred from the presence of corundum with muscovite and K-feldspar, rare presence of spinel overgrowing corundum, and the absence of diaspore, margarite, and dolomite. Because the marble is almost pure calcite (dolomite is very rare), the corundum was preserved because it did not react with dolomite to spinel + calcite during decompression. In some cases, breakdown of muscovite together with rare dolomite probably took place, producing corundum (type III), phlogopite, calcite, and fluids. We assume that the system retained high X_{CO2} during the prograde stage and part of the decompression, until the influx of scapolite-forming fluids.

The observed mineral assemblages resulted from non-ideal stoichiometry of the reacting phases. When the dehydration curve for muscovite + calcite is calculated using the electron microprobe analysis of the muscovite from the muscovite–anorthite–K-feldspar aggregates in association with corundum, the resulting stable mineral assemblage is consistent with those observed in thin sections:

Mg,Ti-bearing muscovite + K-feldspar + anorthite + calcite + H_2O + CO_2 ↔ K-feldspar + phlogopite + anorthite + rutile + corundum + calcite + H_2O + CO_2.

The model results indicate minor formation of anorthite in the corundum stability field. It explains the presence of the rare anorthite + corundum assemblage (Fig. 4E). This corundum-forming reaction takes place at the same P–T conditions as when calculated using the theoretical muscovite formula.

11.5. Retrograde fluids

The occurrence of scapolite, retrograde alteration of diopside, feldspars and corundum, and the breakdown of titanite in mica-feldspar layers all indicate the presence of retrograde fluids. Although most of the alteration features can be attributed to hydration of the system during decompression and cooling, the presence of scapolite indicates high salinity of fluids at relatively high temperature. For the observed scapolite composition, most authors estimate its origin in the range 600–750 °C and pressure ~2–5 kbar (Ellis, 1978; Piazolo and Markl, 1999). At the Revelstoke occurrence, these P–T conditions correspond with the end of decompression and their validity is supported by the late origin of scapolite, after formation of feldspars, micas and corundum. Scapolite in the marble formed after the crystallization of corundum, by the replacement of anorthite and calcite by saline fluids.

The NaCl content of the late fluids was estimated from the scapolite compositions using the experimental data of Ellis (1978) for 4 kbar and 750 °C (cf. Markl and Piazolo, 1998). The experimental data assume only NaCl–H_2O fluid without CO_2; therefore, the results should be regarded as rough estimations of the maximum contents of NaCl in the fluids (for detailed discussion see Markl and Piazolo, 1998; Mora and Valley, 1989). The estimated NaCl/(NaCl + H_2O) ratio varies between 0.05 and 0.3 for most of the data, corresponding to ~15 to 58 wt.% NaCl present in the fluid; the highest marialite compositions in the garnet assemblage in the marble indicate the presence of highly saline fluids with the ratio NaCl/(NaCl + H_2O) up to 0.5 (~76 wt.% NaCl). Although similar values are reported for evaporite brines, the source of high Na and Cl contents in the Revelstoke marble is not clear. The only Cl- or Na-bearing phases are apatite, scapolite, amphiboles and late albite in alteration products; the origin of the amphiboles and albite can be related to the scapolite-forming saline fluids, but apatite appears to be one of the earliest primary minerals in the marble. The Cl- and S-absent composition of scapolite from the host rock indicates low salinity of fluids at peak metamorphic conditions; therefore, the fluids must have been derived from an isolated external source or by dissolution of speculative evaporite beds in the marble.

Scapolite in the marble and in the host rock is typically accompanied by crack-filling sulfide mineralization. The sulfide minerals in the host rock are commonly concentrated in fractures along foliation planes and in retrograde assemblages, especially those replacing garnet porphyroblasts. The scapolite is always free of $(SO_4)^{2-}$ and it does not contain sulfide inclusions; hence, the sulfide mineralization likely represents a different stage of fluid flow.

Occurrences of tourmaline in both marble and gneiss indicate the presence of Na,B-bearing retrograde fluids. The low Ca contents in tourmaline suggest low X_{Ca} of fluids in the marble (von Goerne et al., 2011); the rimwards increase of Ca and F in the gneiss tourmaline indicates their fractionation in the residual metamorphic fluid.

Replacement of clinopyroxene by tremolite, calcite and quartz by the reaction

5 diopside + H_2O + $3CO_2$ → tremolite + 3 calcite + 2 quartz

took place below ~550 °C at 4 kbar (Fig. 12a); its low Na-contents suggest significant removal of NaCl, either due to fractionation or mixing of the fluids with an external low-saline source. At approximately the same temperature, low-saline fluids altered primary minerals in the marble assemblages; replacement of corundum and anorthite, scapolite and K-feldspar by margarite and muscovite took place at ~520–550 °C (Fig. 12b). Further late fluid-driven reactions also include chloritization of biotite, sericitization of feldspars, and veinlets of Fe-oxides.

Graphite in the marble mineral assemblages usually occurs as fissure filling and coats and rims both prograde and retrograde minerals. We assume that it precipitated from late retrograde fluids during cooling and during cataclasis of the rock at low temperature during brittle deformation in the marble.

Retrograde deformation of the marble associated with fluid-assisted recrystallization of calcite and other minerals (e.g. scapolitization) caused thinning and disaggregation of the mica-feldspar layers (cf., Fig. 2B) and locally also separation of corundum crystals from the aggregates with micas and feldspars. The isolated gemmy euhedral corundum crystals found in a coarser calcite in the Zone 3 can be therefore explained by detachment of the crystals from their original assemblage on borders of muscovite–feldspar aggregates.

11.6. Comparison to other deposits

Different models have been used to explain corundum formation in carbonate rocks (e.g., Giuliani et al., 2007). The Revelstoke deposit shares some common features with other ruby deposits from central and southeast Asia (Garnier et al., 2008) including: "(1) they are hosted

by metamorphosed marine carbonates (within gneisses); (2) they formed during amphibolite to lower granulite facies metamorphism; (3) ruby has no relationship with dikes or pegmatites; and (4) the ruby-bearing marbles contain scattered ruby mineralization which is concordant with the surrounding stratigraphic units." Moreover, the corundum assemblages were affected by highly saline retrograde fluids producing scapolite, which is a typical feature of south-Asian gem corundum deposits (Garnier et al., 2008).

However, numerous differences exist between the Revelstoke occurrence and other localities including the corundum-bearing mineral assemblages, mineral and fluid inclusions in corundum, oxygen isotopes of corundum and marble, and the quality and intensity of color of corundum crystals. Most importantly, the Revelstoke corundum formed by prograde muscovite breakdown at high pressure, whereas the Asian rubies are the product of retrograde low pressure breakdown of spinel.

At the south-Asian ruby deposits, Garnier et al. (2008) observed the following which are not present at Revelstoke: (1) corundum formation by the breakdown of spinel during retrograde metamorphism; (2) Na,S, B mineralization (tourmaline, aspidolite, pargasite, edenite, anhydrite) and Mg mineralization (chlorite and sapphirine) associated with corundum; (3) fluid inclusions in corundum with the composition of COS–S_8–AlO(OH); and (4) inclusions of anhydrite and salts in corundum. In contrast, at the Revelstoke occurrence corundum formed prior to spinel by prograde muscovite dehydration and the Na, S and B minerals are either not directly associated with ruby (pargasite, hastingsite, edenite, tourmaline) or clearly post-date its formation (scapolite, sulfide minerals). The scapolite associated with corundum is also sulfur-free and poor in Na (~0.75–1.5 apfu in scapolite) and Cl (usually <0.3 apfu Cl in scapolite). Even though we did not see evidence for anhydrite or COS–S_8–AlO(OH) fluid inclusions in corundum, we cannot discount that they exist. Although the brines responsible for formation of scapolite could have originated from evaporite pods in the rock, it was volumetrically insignificant compared to the siliciclastic component. This is expressed by the lower values of oxygen isotopes for corundum and marble minerals and the scarcity of Na,S,B-mineralization, which differ significantly from those observed by Garnier et al. (2008).

12. Summary

This study has contributed to both the petrology of metasediments in the Frenchman Cap dome as well as the formation of gem corundum in carbonate rocks during prograde metamorphism and metasomatism of pelitic layers within marble. Whole rock geochemistry data indicate that the corundum-bearing silicate (mica-feldspar) layers formed by the mechanical mixing of carbonate with the protolith of the host gneiss. The silicate layers and the gneiss contain elevated contents of V and Cr due to the presence of a volcanoclastic component in their protolith. The bulk composition of the silicate layers was then depleted in Si and Fe during prograde metamorphism; the Si and Fe depletion was enhanced by extensive fluid–rock interaction which resulted in the homogenization of $\delta^{18}O$ and $\delta^{13}C$ values in carbonates and silicates in the marble and silicate layers as well as low $\delta^{18}O$ in corundum.

Corundum occurs in thin, folded and stretched layers with green muscovite + Ba-bearing K-feldspar + anorthite ($An_{0.85-1}$) ± phlogopite ± Na-poor scapolite. Gem corundum was produced in the mica-feldspar layers by mica dehydration at the peak of metamorphism (~650–700 °C at 8.5–9 kbar) following a clockwise P–T path. Fluid inclusions in corundum are pure CO_2 indicating the presence of a CO_2-rich fluid during corundum formation. Because the marble is almost pure calcite (dolomite is very rare), the corundum was preserved because it did not react with dolomite to spinel + calcite during decompression. The micas associated with corundum in the mica-feldspar layers have elevated Ti, V and Cr indicating that they were the source of Ti, V and Cr in the corundum crystals. The mica-feldspar layers were an ideal environment for corundum formation because of the lack of Si and Fe, and enrichment of Ti, V and Cr.

Gem-quality corundum crystals formed especially on borders of the mica-feldspar layers in an assemblage with calcite. Retrograde deformation and fluid-assisted recrystallization of the marble sometimes caused separation of the corundum crystals from their original silicate assemblages.

Acknowledgements

The authors would like to thank Brad Wilson for access to the locality and providing selected samples. Financial support was provided by the Natural Sciences and Engineering Research Council of Canada in the form of a Discovery Grants to L.A.G. and G.M.D., by the Ministry of Culture of the Czech Republic (as part of its long-term conceptual development program for research institutions, the Moravian Museum, MK000094862) to J.C., and by the Society of Economic Geologists and Geoscience B.C. to T.J.D.

Appendices A, B, C. Supplementary data

Supplementary data to this article can be found online at http://dx.doi.org/10.1016/j.lithos.2014.03.030.

References

Bačík, P., Méres, S., Uher, P., 2011. Vanandium-bearing tourmaline in metacherts from Chvojnica, Slovak Republic: crystal chemistry and multistage evolution. Canadian Mineralogist 49, 195–206.
Bačík, P., Uher, P., Cempírek, J., Vaculovič, T., 2012. Magnesian tourmalines from plagioclase–muscovite–scapolite metaevaporite layers in dolomite marble near Prosetín (Olešnice Unit, Moravicum, Czech Republic). Journal of Geosciences 57, 143–153.
Barker, S.L.L., Dipple, G.M., Dong, F., Baer, D.S., 2011. Use of laser spectroscopy to measure the $^{13}C/^{12}C$ and $^{18}O/^{16}O$ compositions of carbonate minerals. Analytical Chemistry 83, 2220–2226.
Baxter, E.F., 2010. Diffusion of noble gases in minerals. Reviews in Mineralogy and Geochemistry 72, 509–557.
Bhattacharya, A., Mohanty, L., Maji, A., Sen, S.K., Raith, M., 1992. Non-ideal mixing in the phlogopite–annite binary: constraints from experimental data on Mg–Fe partitioning and a reformulation of the biotite–garnet thermometer. Contributions to Mineralogy and Petrology 111, 87–93.
Bol, L.C.G.M., Bos, A., Sauter, C.C., Jansen, J.B.H., 1989. Barium–titanium-rich phlogopites in marbles from Rogaland, southwest Norway. American Mineralogist 74, 439–447.
Bowman, J.R., 1998. Stable-isotope systematics of skarns. In: Lentz, D.R. (Ed.), Mineralized Intrusion-related Skarn Systems. Mineralogical Association of Canada Short Course, vol. 26, pp. 99–145.
Brady, J.B., 1977. Metasomatic zones in metamorphic rocks. Geochimica et Cosmochimica Acta 41, 113–125.
Breit, G.N., Wanty, R.B., 1991. Vanadium accumulation in carbonaceous rocks: a review of geochemical controls during deposition and diagenesis. Chemical Geology 91, 83–97.
Brown, R.L., 1980. Frenchman Cap Dome, Shuswap Complex, British Columbia: a progress report. Current Research, Part A, Geological Survey of Canada, Paper 80, pp. 47–51.
Brown, R.L., Journeay, J.M., Lane, L.S., Murphy, D.C., Rees, C.J., 1986. Obduction, backfolding and piggyback thrusting in the metamorphic hinterland of the southeastern Canadian Cordillera. Journal of Structural Geology 8, 225–268.
Canet, C., Alfonso, P., Melgarejo, J.-C., Jorge, S., 2003. V-rich minerals in contact-metamorphosed silurian SEDEX deposits in the Poblet area, southwestern Catalonia, Spain. Canadian Mineralogist 41, 561–579.
Cempírek, J., Houzar, S., Novák, M., 2008. Complexly zoned niobian titanite from hedenbergite skarn at Písek, Czech Republic, constrained by substitutions Al(Nb, Ta)Ti_{-2}, Al(F, OH)$(TiO)_{-1}$ and $SnTi_{-1}$. Mineralogical Magazine 76, 1293–1305.
Cempírek, J., Houzar, S., Novák, M., Groat, L.A., Selway, J.B., Šrein, V., 2013. Crystal structure and compositional evolution of vanadium-rich oxy dravite from graphite quartzite at Bítovánky, Czech Republic. Journal of Geosciences 58, 149–162.
Crowley, J.L., 1999. U–Pb geochronologic constraints on Paleoproterozoic tectonism in the Monashee complex, Canadian Cordillera: elucidating an overprint geologic history. Geological Society of America Bulletin 111, 560–577.
Crowley, J.L., Parrish, R.R., 1999. U–Pb isotopic constraints on diachronous metamorphism in the northern Monashee complex, southern Canadian Cordillera. Journal of Metamorphic Petrology 17, 483–502.
Crowley, J.L., Brown, R.L., Parrish, R.R., 2001. Diachronous deformation and a strain gradient beneath the Selkirk allochthon, northern Monashee complex, southeaster Canadian Cordillera. Journal of Structural Geology 23, 1103–1121.
de Capitani, C., Petrakakis, K., 2010. The computation of equilibrium assemblage diagrams with Theriak/Domino software. American Mineralogist 95, 1006–1016.
Deer, W.A., Howie, R.A., Zussman, J., 2001. Rock Forming Minerals. Framework Silicates: Feldspars. Volume 4ASecond edition. The Geological Society of London.
Doležalová, H., Houzar, S., Losos, Z., Škoda, R., 2006. Kinoshitalite with a high magnesium content in sulphide-rich marbles from the Rožná uranium deposit, Western Moravia, Czech Republic. Neues Jahrbuch für Mineralogie (Abhandlungen) 182, 165–171.

Durstling, H., 2005. New discovery: rubies in Nova Scotia. Canadian Gemmologist 26, 93–94.
Ellis, D.E., 1978. Stability and phase equilibria of chloride and carbonate bearing scapolites at 750 °C and 4000 bar. Geochimica et Cosmochimica Acta 42, 1271–1281.
Garnier, V., Giuliani, G., Ohnenstetter, D., Fallick, A.E., Dubessy, J., Banks, D., Vinh, H.Q., Lhomme, T., Maluski, H., Pêcher, A., Bakhsh, K.A., Van Long, P., Trong Trinh, P., Schwarz, D., 2008. Marble-hosted ruby deposits from Central and Southeast Asia: towards a new genetic model. Ore Geology Reviews 34, 169–191.
Gertzbein, P.J., 2005. Geology surrounding the Beluga sapphire occurrence, Kimmirut, Nunavut: a preliminary examination. Canadian Gemmologist 26, 50–57.
Gervais, F., Brown, R.L., 2011. Testing modes of exhumation in collisional orogens: synconvergent channel flow in the southeastern Canadian Cordillera. Lithosphere 3, 55–75.
Gervais, F., Brown, R.L., Crowley, J.L., 2010. Tectonic implications for a Cordilleran orogenic base in the Frenchman Cap dome, southeastern Canadian Cordillera. Journal of Structural Geology 32, 941–959.
Ghent, E.D., O'Neil, J.R., 1985. Late Precambrian marbles of unusual carbon-isotope composition, southeastern British Columbia. Canadian Journal of Earth Sciences 22, 324–329.
Giuliani, G., Dubessy, J., Banks, D., Hoang Quang, V., Lhomme, T., Pironon, J., Garnier, V., Phan Trong, T., Pham Van, L., Ohnenstetter, D., Schwarz, D., 2003. CO_2–H_2S–COS–S_8 AlO–(OH)-bearing fluid inclusions in ruby from marble-hosted deposits in Luc Yen area, North Vietnam. Chemical Geology 194, 167–185.
Giuliani, G., Fallick, A.E., Garnier, V., France-Lanord, C., Ohnenstetter, D., Schwarz, D., 2005. Oxygen isotope composition as a tracer for the origins of rubies and sapphires. Geology 33, 249–252.
Giuliani, G., Ohnenstetter, D., Garnier, V., Fallick, A.E., Rakotondrazafy, M., Schwarz, D., 2007. The geology and genesis of gem corundum deposits. In: Groat, L.A. (Ed.), Geology of Gem Deposits. Mineralogical Association of Canada Short Course, vol. 37, pp. 23–78.
Grapes, R., Palmer, K., 1996. (Ruby–sapphire)-chromian mica-tourmaline rocks from Westland, New Zealand. Journal of Petrology 37, 293–315.
Groat, L.A., Laurs, B.M., 2009. Gem formation, production, and exploration: why gem deposits are rare and what is being done to find them. Elements 5, 153–158.
Harlov, D., Tropper, P., Seifert, W., Nijland, T., Förster, H.-J., 2006. Formation of Al-rich titanite ($CaTiSiO_4O$–$CaAlSiO_4OH$) reaction rims on ilmenite in metamorphic rocks as a function of fH_2O and fO_2. Lithos 88, 72–84.
Hinchey, A.M., Carr, S.D., McNeill, P.D., Rayner, N., 2006. Paleocene–Eocene high-grade metamorphism, anatexis, and deformation in the Thor–Odin dome, Monashee complex, southeastern British Columbia. Canadian Journal of Earth Science 43, 1341–1365.
Hoefs, J., 2004. Stable Isotope Geochemistry5th edition. Springer, Berlin.
Holk, G.J., Taylor, H.P., 2000. Water as a petrologic catalyst driving $^{18}O/^{16}O$ homogenization and anatexis of the middle crust in the metamorphic core complexes of British Columbia. International Geology Review 42, 97–130.
Houzar, S., Cempírek, J., 2011. Accessory schreyerite in vanadium-rich graphite quartzite at Bítovánky (Moldanubicum, western Moravia). Acta Musei Moraviae, Scientiae Geologicae Paper 96 (2), 35–43 (In Czech with English abstract).
Höy, T., 1987. Geology of the Cottonbelt lead–zinc-magnetite layer, carbonatites and alkalic rocks in the Mount Grace area, Frenchman Cap Dome, southeastern British Columbia. Bulletin — Ministry of Energy, Mines and Petroleum Resources, 80.
Höy, T., 2001. Sedex and Broken Hill-type deposits, northern Monashee mountains, southern British Columbia. British Columbia Geological Survey, Geological Fieldwork 2000. Paper 2001-1, pp. 85–114.
Joesten, R., 1977. Evolution of mineral assemblage zoning in diffusion metasomatism. Geochimica et Cosmochimica Acta 41, 649–670.
Johnson, B.J., 2006. Extensional shear zones, granitic melts, and linkage of overstepping normal faults bounding the Shuswap metamorphic core complex, British Columbia. Geological Society of America Bulletin 118, 366–382.
Journeay, J.M., 1986. Stratigraphy, Internal Strain and Thermo-tectonic Evolution of Northern Frenchman Cap Dome; an Exhumed Duplex Structure, Omineca Hinterland, S. E. Canadian Cordillera. (Ph.D. thesis) Queen's University, Kingston, Ontario.
Krogh, E.J., 1988. The garnet–clinopyroxene Fe–Mg geothermometer — a reinterpretation of existing experimental data. Contributions to Mineralogy and Petrology 99, 44–48.
Kullerud, K., Erambert, M., 1999. Cl-scapolite, Cl-amphibole, and plagioclase equilibria in ductile shear zones at Nusfjord, Lofoten, Norway: implications for fluid compositional evolution during fluid–mineral interaction in the deep crust. Geochimica et Cosmochimica Acta 63, 3829–3844.
Lane, L.S., 1984. Brittle deformation in the Columbia River fault zone near Revelstoke, southeastern British Columbia. Canadian Journal of Earth Sciences 21, 584–598.
Leake, B.E., Woolley, A.R., Birch, W.D., Burke, E.A.J., Ferraris, G., Grice, J.D., Hawthorne, F.C., Kisch, H.J., Krivovichev, V.G., Schumacher, J.C., Stephenson, N.C.N., Whittaker, E.J.W., 2004. Nomenclature of amphiboles: additions and revisions to the International Mineralogical Association's amphibole nomeclature. American Mineralogist 89, 883–887.
LeCheminant, A.N., Groat, L.A., Mortensen, J.K., Gertzbein, P., Rohtert, W., 2005. Sapphires from Kimmirut, Baffin Island, Nunavut, Canada. Geochimica et Cosmochimica Acta 69, A280.
Lee, C.H., Lee, H.K., 2003. Vanadium- and barium-bearing green mica within coaly metapelite from the Ogcheon Supergroup, Republic of Korea. Journal of Asian Earth Sciences 21, 343–351.
Limtrakun, P., Zaw, K., Ryan, C.G., Mernagh, T.P., 2001. Formation of the Denchai gem sapphires, northern Thailand: evidence from mineral chemistry and fluid/melt inclusion characteristics. Mineralogical Magazine 65, 725–735.
Ludwig, K.R., 2003. Isoplot 3.09: a geochronological toolkit for Microsoft Excel. Berkeley Geochronology Center, Special, Publication No. 4.
Manning, C.E., 2007. Solubility of corundum + kyanite in H_2O at 700 °C and 10 kbar: evidence for Al–Si complexing at high pressure and temperature. Geofluids 7, 258–269.
Markl, G., Piazolo, S., 1998. Halogen-bearing minerals in syenites and high-grade marbles of Dronning Maud Land, Antarctica: monitors of fluid compositional changes during late-magmatic fluid–rock interaction processes. Contributions to Mineralogy and Petrology 132, 246–268.
Markl, G., Piazolo, S., 1999. Stability of high-Al titanite from low-pressure calcsilicates in light of fluid and host-rock composition. American Mineralogist 84, 37–47.
Meinert, L.D., Dipple, G.M., Nicolescu, S., 2005. World skarn deposits. In: Hedenquist, J.W., Thompson, J.F.H., Goldfarb, R.J., Richards, J.P. (Eds.), Economic Geology: One Hundredth Anniversary, 1905–2005, pp. 299–336.
Moine, B., Sauvan, P., Jarousse, J., 1981. Geochemistry of evaporite-bearing series: a tentative guide for the identification of metaevaporites. Contributions to Mineralogy and Petrology 76, 401–412.
Mora, C.I., Valley, J.W., 1989. Halogen-rich scapolite and biotite: implication for metamorphic fluid rock interaction. American Mineralogist 74, 721–737.
Norlander, B.H., Whitney, D.L., Teyssier, C., Vanderhaeghe, O., 2002. Partial melting and decompression of the Thor–Odin dome, Shuswap metamorphic complex, Canadian Cordillera. Lithos 61, 103–125.
Pak, T.M., Hauzenberger, C.A., Baumgartner, L.P., 2003. Solubility of the assemblage albite + K-feldspar + andalusite + quartz in supercritical aqueous chloride solutions at 650 °C and 2 kbar. Chemical Geology 200, 377–393.
Pan, Y., Fleet, M.E., 1991. Barian feldspar and barian–chromian muscovite from the Hemlo area, Ontario. Canadian Mineralogist 29, 481–498.
Pan, Y., Fleet, M.E., Ray, G.E., 1994. Scapolite in two Canadian gold deposits: Nickel Plate, British Columbia and Hemlo, Ontario. Canadian Mineralogist 32, 825–837.
Piazolo, S., Markl, G., 1999. Humite- and scapolite-bearing assemblages in marbles and calcsilicates of Dronning Maud Land, Antarctica: new data for Gondwana reconstructions. Journal of Metamorphic Petrology 17, 91–107.
Pouchou, J.L., Pichoir, F., 1985. PAP φ(ρZ) procedure for improved quantitative microanalysis. Microbeam Analysis 1985, 104–106.
Read, P.B., Brown, R.L., 1981. Columbia River fault zone: southeastern margin of the Shuswap and Monashee complexes, southeastern British Columbia. Canadian Journal of Earth Sciences 18, 1127–1145.
Renne, P.R., Swisher, C.C., Deino, A.L., Karner, D.B., Owens, T., DePaolo, D.J., 1998. Intercalibration of standards, absolute ages and uncertainties in $^{40}Ar/^{39}Ar$ dating. Chemical Geology 145, 117–152.
Rubatto, D., Müntener, O., Barnhoorn, A., Gregory, C., 2008. Dissolution–reprecipitation of zircon at low-temperature, high-pressure conditions (Lanzo Massif, Italy). American Mineralogist 93, 1519–1529.
Sanborn, N.M., 1996. Constraints on the Timing and Conditions of Cordilleran Tectonism in Frenchman Cap Dome, Monashee Complex, Southeast British Columbia, From $^{40}Ar/^{39}Ar$ Geochronology. (BSc Thesis) Queens University, Kingston, Ontario, Canada.
Seward, T.M., 1974. Determination of the first ionization constant of silicic acid from quartz solubility in borate buffer solutions to 350 °C. Geochimica et Cosmochimica Acta 38, 1651–1664.
Shannon, R.D., 1976. Revised effective ionic radii and systematic studies of interatomic distances in halides and chalcogenides. Acta Crystallographica A32, 751–767.
Shor, R., Weldon, R., 2009. Ruby and sapphire production and distribution: a quarter century of change. Gems and Gemology 45, 236–259.
Simonet, C., Fritsch, E., Lasnier, B., 2008. A classification of gem corundum deposits aimed towards gem exploration. Ore Geology Reviews 34, 127–133.
Snetsinger, K.G., 1966. Barium–vanadium muscovite and vanadium tourmaline from Mariposa County, California. American Mineralogist 51, 1623–1639.
Spear, F.S., Kohn, M.J., Cheney, J.T., 1999. *P–T* paths from anatectic pelites. Contributions to Mineralogy and Petrology 134, 17–32.
Sun, S.-s, McDonough, W.F., 1989. Chemical and isotopic systematics of oceanic basalts: implications for mantle composition and processes. Geological Society, London, Special Publications 42, 313–345.
Takayuki, S., Sasaki, M., Fujimoto, K., Takeno, N., Tsukamoto, H., Sanada, K., Maeda, S., 2001. Corundum and zincian spinel from the Kakkonda geothermal system, Iwate Prefecture, northeastern Japan. Journal of Mineralogical and Petrological Sciences 96, 137–147.
Teyssier, C., Ferré, E., Whitney, D.L., Norlander, B., Vanderhaeghe, O., Parkinson, D., 2005. Flow of partially molten crust and origin of detachments during collapse of the Cordilleran orogen. Geological Society, London, Special Publications 245, 39–64.
Treloar, P.J., 1987. The Cr-minerals of Outokumpu — their chemistry and significance. Journal of Petrology 28, 867–886.
Tropper, P., Manning, C.E., Essene, E.J., 2002. The substitution of Al and F in titanite at high pressure and temperature: experimental constraints on phase relations and solid solution properties. Journal of Petrology 43, 1787–1814.
Uher, P., Kováčik, M., Kubiš, M., Shtukenberg, A., Ozdín, D., 2008. Metamorphic vanadian–chromian silicate mineralization in carbon-rich amphibole schists from the Malé Karpaty Mountains, Western Carpathians, Slovakia. American Mineralogist 93, 63–73.
Uvarova, Y.A., Kyser, T.K., Sokolova, E., Kazansky, V.I., Lobanov, K.V., 2011. Significance of stable isotope variations in crustal rocks from the Kola Superdeep Borehole and their surface analogues. Precambrian Research 189, 104–113.
Valley, J.W., 1986. Stable isotope geochemistry of metamorphic rocks. Reviews in Mineralogy and Geochemistry 16, 445–489.
Van den Kerkhof, A., Thiéry, R., 2001. Carbonic inclusions. Lithos 55, 49–68.
von Goerne, G., Franz, G., van Hinsberg, V.J., 2011. Experimental determination of Na–Ca distribution between tourmaline and fluid in the system CaO–Na_2O–MgO–Al_2O_3–SiO_2–B_2O_3–H_2O. Canadian Mineralogist 49, 137–152.

Walther, J.V., Woodland, A.B., 1993. Experimental determination and interpretation of the solubility of the assemblage microcline, muscovite, and quartz in supercritical H_2O. Geochimica et Cosmochimica Acta 57, 2431–2437.
Whitney, D.L., Evans, B.W., 2010. Abbreviations for names of rock-forming minerals. American Mineralogist 95, 185–187.
Wight, W., 1999. Explosion of new interest in Canadian gemstones. Canadian Gemmologist 20, 45–53.
Wight, W., 2004. Sapphire from Ontario. Canadian Gemmologist 25, 30–32.
Wilson, B., 2010. Colored gemstones from Canada. Rocks and Minerals 85, 24–43.